International Journal of Architectural Heritage
Conservation, Analysis, and Restoration

ISSN: 1558-3058 (Print) 1558-3066 (Online) Journal homepage: http://www.tandfonline.com/loi/uarc20

Structural Characterization and Seismic Performance of San Francisco Church, the Most Ancient Monument in Santiago, Chile

Natalia Jorquera, Giulia Misseri, Nuria Palazzi, Luisa Rovero & Ugo Tonietti

To cite this article: Natalia Jorquera, Giulia Misseri, Nuria Palazzi, Luisa Rovero & Ugo Tonietti (2017) Structural Characterization and Seismic Performance of San Francisco Church, the Most Ancient Monument in Santiago, Chile, International Journal of Architectural Heritage, 11:8, 1061-1085, DOI: 10.1080/15583058.2017.1315620

To link to this article: https://doi.org/10.1080/15583058.2017.1315620

Accepted author version posted online: 06 Jun 2017.
Published online: 05 Oct 2017.

INTERNATIONAL JOURNAL OF ARCHITECTURAL HERITAGE
2017, VOL. 11, NO. 8, 1061–1085
https://doi.org/10.1080/15583058.2017.1315620

Structural Characterization and Seismic Performance of San Francisco Church, the Most Ancient Monument in Santiago, Chile

Natalia Jorquera[a], Giulia Misseri[b], Nuria Palazzi[b], Luisa Rovero[b], and Ugo Tonietti[b]

[a]Department of Architecture, Universidad de Chile, Santiago, Chile; [b]Department of Architecture, University of Florence, Florence, Italy

ABSTRACT

The Church of San Francisco is the oldest religious building in use in Chile and an iconic and historical heritage landmark of the capital Santiago. The church, the result of joint work between the Spanish and local indigenous people, was built in stone and brick masonry and has been modified by additions and constructive changes since its construction in 1586. The building has shown a remarkable resilience, withstanding about 15 destructive earthquakes.

As part of research whose goal is to discover the basis of the structural behavior of the church, in this article a safety assessment of the monument is carried out based on a multi-disciplinary approach. Main fields comprises historical research, in situ surveys, crack pattern analysis, physical and mechanical characterization of materials, and multi-level structural analyses. The results highlight the particularities of the building and the current seismic vulnerabilities in order to provide a robust knowledge basis on which possibly pivoting future consolidation and safeguarding strategies could be done.

ARTICLE HISTORY
Received 6 October 2016
Accepted 1 April 2017

KEYWORDS
Chilean colonial architecture; cultural heritage; masonry building techniques; San Francisco church; seismic vulnerability assessment; structural behavior

1. Introduction

The church of San Francisco has a basilica plan with three aisles (Figure 1) and is flanked by an adobe building that houses the convent. The church is the oldest building in Santiago and the only surviving authentic architectural testimony of the sixteenth century in Chile (Benavides 1988[1941], p. 128). The church has survived to about 15 earthquakes of magnitude between 7.1 and 9.5 (Chilean National Seismological Centro, http://sismologia.cl/ [accessed 10 October 2015]; Astroza et al. 2010), most of them with epicenters far away from Santiago but nevertheless experienced with intensities from strong to severe levels in the city provoking damages to many buildings. During all these earthquakes the church has suffered several local damages which can be perceived in the evident repairs or changes of building materials. However, there is poor information about such damages.

In Pena (1969) a broader, although incomplete, gathering of information about the evolution of the church is reported. Further information about the construction phases of San Francisco is provided in Pereira Salas (1965), Benavides (1988[1941]), Villalobos et al. (1990), De Ramón (2000), Rovegno (2009), Sahady (2015), and Gross (2015).

The study of San Francisco church is relevant because it is an entirely unique case in Chile of a transition building in which still coexist clear typological elements of the Andean building culture and the architectural elements established in the 17th century of colonial architecture.

Furthermore, the construction technology features enforcing the significant structural resilience of the building have not been fully investigated both in the light of the high seismic hazard of the Chilean context and of the use of constructive techniques which the church is built with. For these reasons, a complete analysis of San Francisco has been carried out using methodologies for the structural analysis of heritage buildings already proposed and validated (Fratini et al. 2011; Gamrani et al. 2012; Rovero and Fratini 2013; Rovero and Tonietti 2012, 2014; Sani et al. 2012). As a general framework, a multi-level approach, comprising historical research, in situ surveys, crack pattern analysis, physical and mechanical characterization of materials and local and global structural analysis, has been adopted. This article is organized into seven sections, including the Introduction. The second and third sections describe the construction phases and characteristics of the building; the fourth section is

CONTACT Natalia Jorquera nataliajorquera@uchilefau.cl Department of Architecture, Universidad de Chile, Portugal 84, 1025000 Santiago, Chile.
Color versions of one or more of the figures in the article can be found online at www.tandfonline.com/UARC.

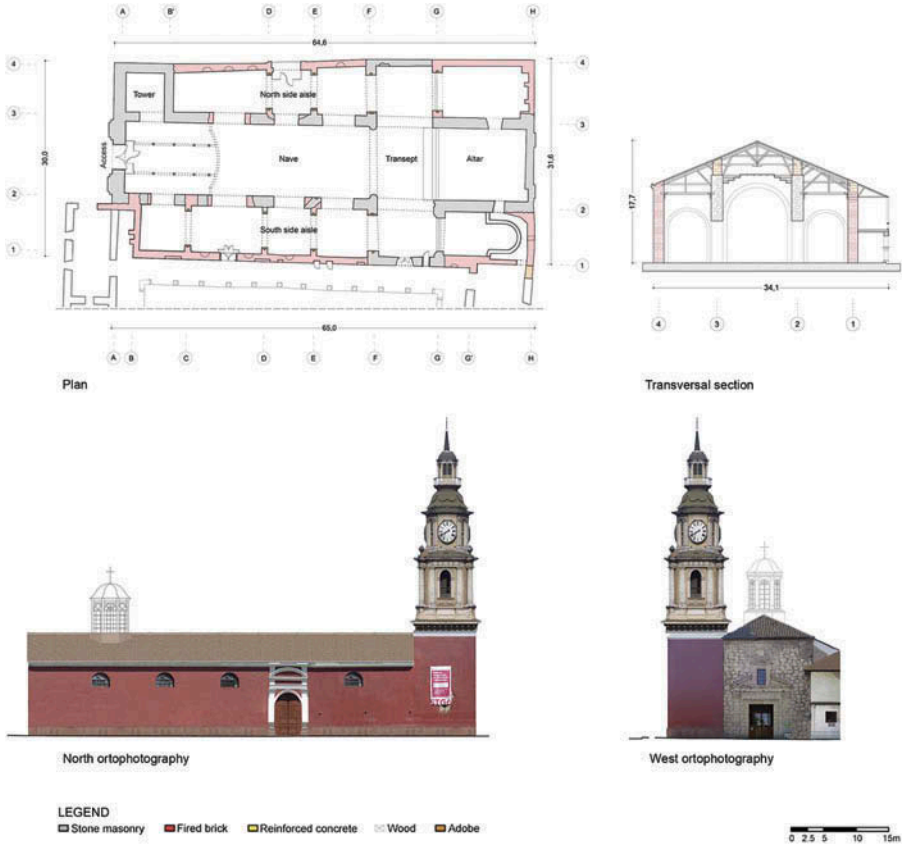

Figure 1. Plans, section and elevations of San Francisco in its current state, with information of the main building materials.

dedicated to essays and tests aimed at the characterization of materials. The fifth and sixth sections are dedicated to crack pattern assessment and to the structural analysis.

2. Construction phases

Throughout its 400 years of history, the church of San Francisco has had many transformations: additions of parts due to enlargement needs, stylistic modifications, and repairs of damages after earthquakes. However, the church has never experienced complete collapsed, thus it has never been demolished, and has always remained in use. Each transformation was made using the building technologies of the corresponding historical period. In the case of repairs, no operations of anastylosis have been reported, but integrations of clearly differentiated parts.

According to the historiographical information (Benavides 1988[1941]; De Ramón 2000; Gross 2015; Pena 1969; Pereira Salas 1965; Rovegno 2009; Sahady 2015; Villalobos et al. 1990) and through visual inspections of the areas characterized by structural discontinuity and inhomogeneity of materials, five main construction phases can be recognized (Figure 2).

The first phase corresponds to the period of construction of the church (1586–1618) and the earthquake of 1647. This church was characterized by a Latin cross plan, two

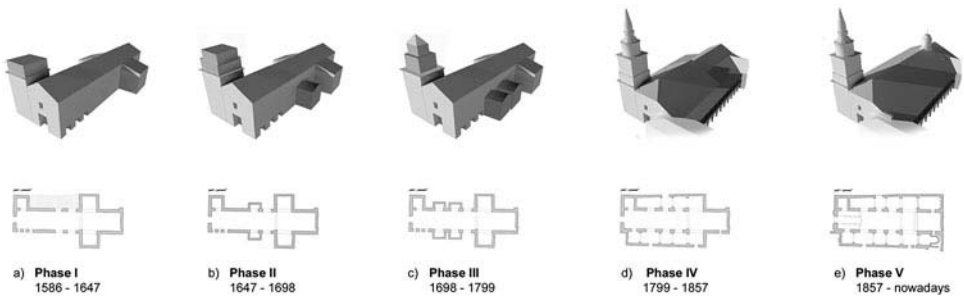

Figure 2. Constructive phases and architectural changes of San Francisco since 1586 to the present.

lateral chapels and a bell tower attached to the main façade (Figure 2a), all built completely in rubble cyclopean stone masonry. Because of the constructive and typological features, this first part of the church shows a strong familiarity with the vernacular Andean churches of the north of Chile and Argentina and the south of Peru and Bolivia representative of Andean building culture (Figure 3a). In fact, the Latin cross plan, the bell tower at the side of the main façade, the lateral chapels, which work as buttresses of the longitudinal walls (Figure 3b), and the cyclopean masonry texture with stones and earth mortar (Figure 3c), are all recurring motifs in the Andean churches (Benavides, Marquez de la Plata, and Rodriguez 1977; Jorquera 2010; Montandón 1950; Rodríguez 2012). This undeniable influence, detectable in the tangible evidence presented in San Francisco, is further strengthened by witness accounts documenting the use of Andean workforce, including indigenous and people of dual ethnic heritage (Pena 1969).

The second construction phase (1647–1698) is characterized by the *Magnum earthquake* of 1647 of estimated magnitude 8 (Lomnitz 2004), considered to have been the most destructive earthquake of the Colonial period. During the earthquake the church lost its tower and part of its choir, while the walls and the roof did not suffer any structural damage (De Ramón 2000), making San Francisco the only surviving building in the whole city of Santiago. In 1684, two lateral chapels were added to the original Latin cross plan, changing the original morphology of the building (Figure 2b). In 1698, the bell tower was rebuilt, however, neither information about the building technologies nor the architectural features of this tower are reported in historical accounts.

Enlargements and reconstructions characterize the third construction phase (1698–1799) (Figure 2c). In this period, the church survived two major earthquakes: one in 1730 of a estimated magnitude between 8.5 and 9 (Lomnitz 2004)—the second most destructive of the Colonial period—without suffering serious damage; and one in 1751 (magnitude 8.5) (Lomnitz 2004), which damaged the bell tower. In 1754, the unstable upper portion of the tower was demolished and rebuilt in brick masonry with an eclectic spirit pulling together three different styles (Rovegno 2009). In 1779, new chapels were built (Rovegno 2009) attached to the main nave, bringing the total number of chapels to eight. In addition, the access to the church was moved from the north aisle wall to the current position along the west façade.

In the fourth construction phase (1799–1857) (Figure 2d), the 1822 earthquake of magnitude 8.0–8.5 (Lomnitz 2004) in La Ligua (Valparaíso) lead to the damage of two arches of the longitudinal nave and part of the roof (Gazeta Ministerial de Chile 1966). In 1825, these two arches were rebuilt in brick, and part of the presbytery behind the wall and the end chapel of south aisle were repaired (De Ramón 2000). Due to the Huasco earthquake of 1851 (magnitude 7.5) (Lomnitz 2004), the top of the tower was again damaged and was replaced in 1857 (De Ramón 2000) by the current wooden belfry to reduce inertial load and guarantee a better seismic performance. The wooden framework was designed by the famous Chilean architect Fermin Vivaceta, who also unified the chapels transforming them into brickwork lateral aisles. With this last intervention the church found its basilica plan. Because of the height of this tower (46.4 m) the building became an urban landmark in the city of Santiago.

During the last construction phase (1857–today), the roof structure was unified, and a new brickwork chapel was added to the eastern part of the church behind the

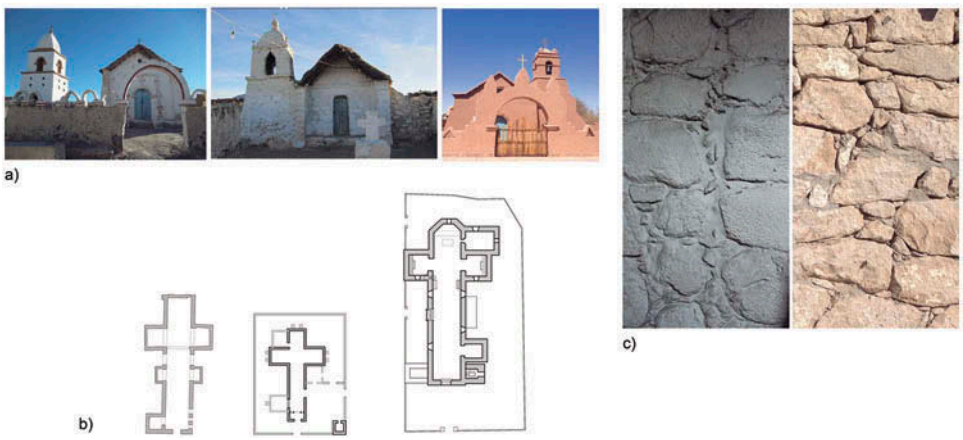

Figure 3. Andean churches. a) Chilean Andean churches of Cotasaya, Guacollo and San Pedro de Atacama, b) Plans of the churches of San Francisco (first phase), Chiu-chiu (first phase) and San Pedro de Atacama, and c) Comparison between the stone masonry of San Francisco church and the Andean church of Caspana.

altar in 1895. In this way, the church acquired its current volumetric configuration (Figure 2e).

In 1951, the Chilean government included the church a in the listed national monuments and during the 90s considered it for nomination in the World Heritage Tentative List to ask in a future for inscription as an UNESCO World Heritage Monument.

In 1985, an earthquake of a magnitude of Mw 8.0, which had its epicentre offshore Valparaiso, was felt in Santiago at 7.5MMI (USGS; http://www.usgs.gov/ [accessed July 13, 2017]). The church suffered extended damages in the transverse arches of lateral aisles, which were then reinforced in 1988 (intervention designed by the engineer Santiago Arias (CMN 2010)) inserting a RC frame (30x30 cm) and a mixed RC-steel tie-rod above the arches (Figure 4). Like most structural interventions on historical monuments after the earthquake of 1985, this reinforcement of San Francisco did not follow any principle of heritage conservation, because of the absence of guidelines for interventions on historical masonry buildings. After the 2010 earthquake of magnitude Mw 8.8 (7.0 MMI in Santiago; Atkinson and Wald 2007), the church presented significant damages, i.e., the displacement of the intrados of arches, some deep cracks in the longitudinal stone walls and walls bulging at spring level of the transverse arches. This pattern of cracks is still visible. In 2015, with Illapel earthquake (Mw 8.3 and MMI 5.3–5.6 in Santiago; Atkinson and Wald 2007)), the pattern of damage of the 2010 earthquake did not significantly worsen.

3. Architectural elements and constructive features

The church has a basilica plan that covers 64.6 m in length and 30.3 m in width, with lateral aisles partitioned by five transverse arcade walls (Figure 5). Roof height spans between 9 and 18 m and the top of tower bell, at 46.4 m, clearly marks the skyline of the city.

The church has underwent several alterations over centuries so that various construction systems and materials are distinguishable. The original portions of the central nave walls are in rubble stone masonry and are 1.65 m thick; on the top of these longitudinal walls, some courses of adobe masonry were added to increase the wall height when the roof structure was unified. The walls of lateral naves are 1 mt thick brickwork along North and South perimeter. The lower part of the main façade, 1.85 m thickness, belongs to the first construction phase and is built in stone masonry, while the top of it was rebuilt in bricks and adobe as the result of repairs after past earthquakes. In the same way, the wall behind the altar, 1.7 m thick, is made of stone masonry and it presents some bricks and adobe courses and a wooden frame at the top as a testimony of ancient earthquakes damage and subsequent repairs.

Along the longitudinal partition walls, two arcades uphold the spatial connection between central and lateral aisles. Among these arches, those of the transept as

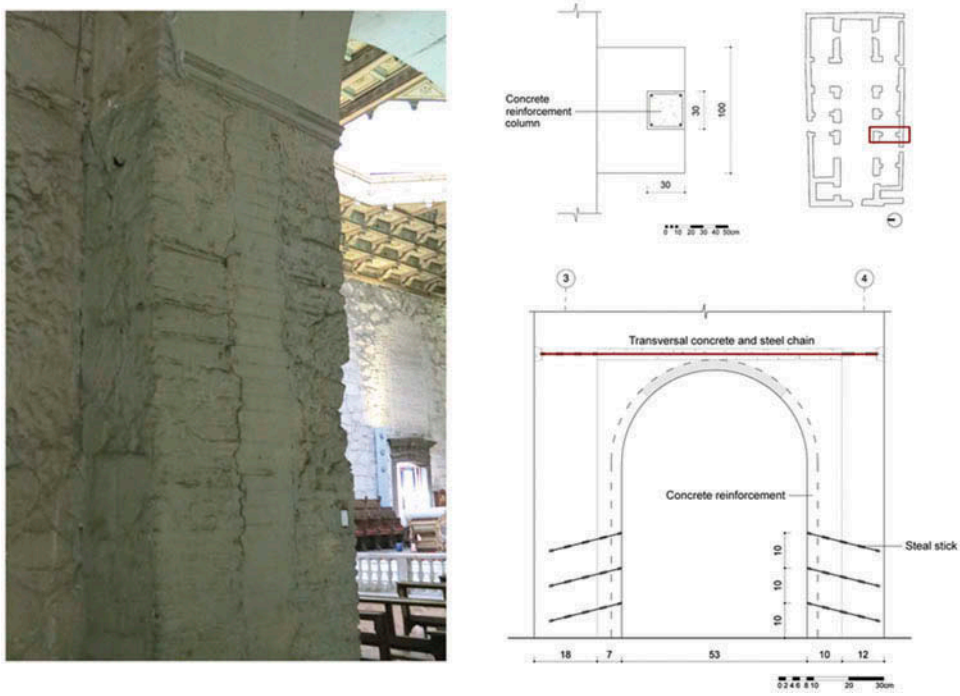

Figure 4. Reinforced Concrete frame reinforcements of transverse arcades walls, 1988 (Plans based on—).

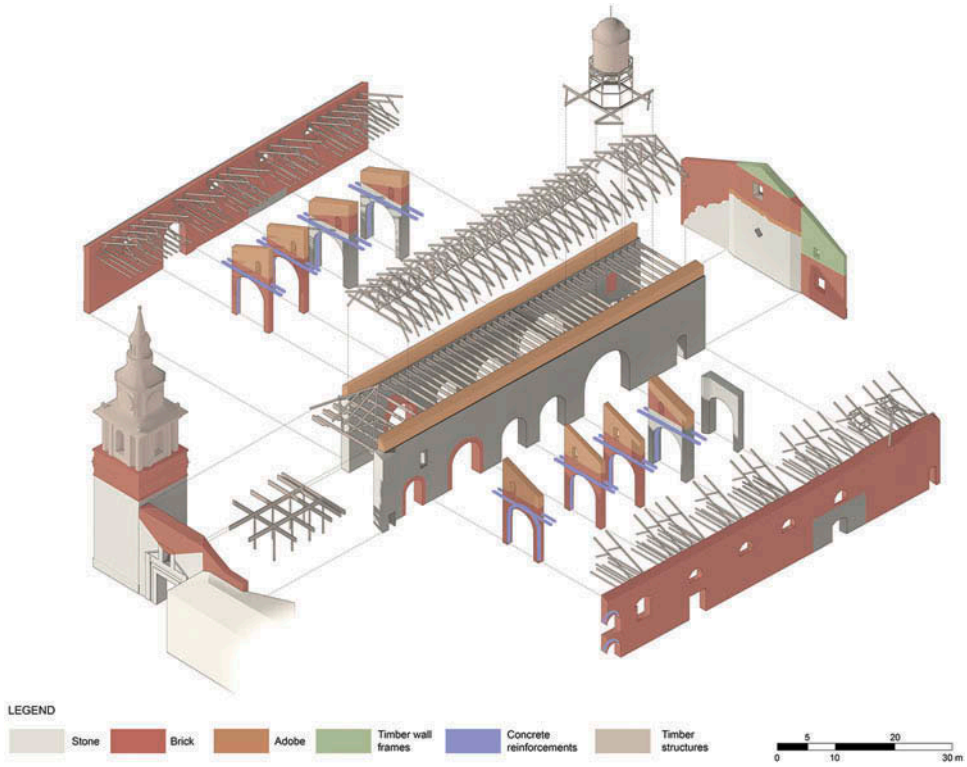

Figure 5. Exploded Axonometric of resistant structure.

well as the adjacent ones are original and built in stone masonry, while the arches near the façade were built in brick together with the lateral aisles (Figure 5 and Figure 1, plan B2-C2); the access arch to the tower (Figure 1, plan B3) is original and made in stone. The five transverse arcades that partition lateral aisles are brick masonries and are reinforced with an RC frame casted within the intrados and an RC-steel tie-rod at the top (Figure 4).

The tower is divided into three bodies built with different materials from the base to the top: the base is rubble stone masonry and belongs to the original part of the church; the second part is built in bricks, and the third part is assembled as a wooden frame of *Olivillo* (*Aextoxicon punctatum*) and Oak (*Nothofagus sp.*). The second and third parts constitute an independent volume 30 m high.

There is no historical information regarding the foundations of the buildings but a 4 m long excavation near the transept, carried out as part of the present research in collaboration with a team of archaeologists, revealed a special system of foundation. This comprises of round river boulders under the walls—with variable dimensions between 10–30 cm—placed without mortar and contained laterally by a course of large and hewed stones of dimension of around 60x60x60 cm with a larger stone in the corner of 90x60x60 cm. Thus, during an earthquake, the stones can move but not scatter laterally thanks to the axis, partially isolating the building from the seismic action (Figure 6).

Since its origin, the church was equipped with a strong horizontal "diaphragm", placed on the central nave under the roof (Figure 7; see also Figures 5, 10, and 14). This system comprises of a series of big cypress (*Austrocedrus chilensis*) wooden beams (30x35 cm cross section) well connected to the walls and placed with 1.2 m spacing that widens to 2 m close to the façade proving a reconstruction intervention, (De Ramón 2000). This original structure still exists today even if it has been partially modified to accomodate the roof lantern that lights up the space over the altar.

The roof structure is constituted by a sequence of wooden trusses (spacing 2.4 m); they are placed above each aisle separately and are located on the top of the adobe walls. The central truss consist of many diagonals and two horizontal beams, where the lower beam traverses the top of the walls partially. The lateral oak (*Nothofagus sp.*) trusses (interaxes about 3 m), much more slender, are formed by one horizontal beam, some diagonals and a vertical chain that connects the trusses to the diaphragm. At roof level, the triangular adobe wall at the top of the transverse walls represents a sort of buttresses for the longitudinal walls and, furthermore a support of the roof. The roof structure is covered by cane and clay tiles.

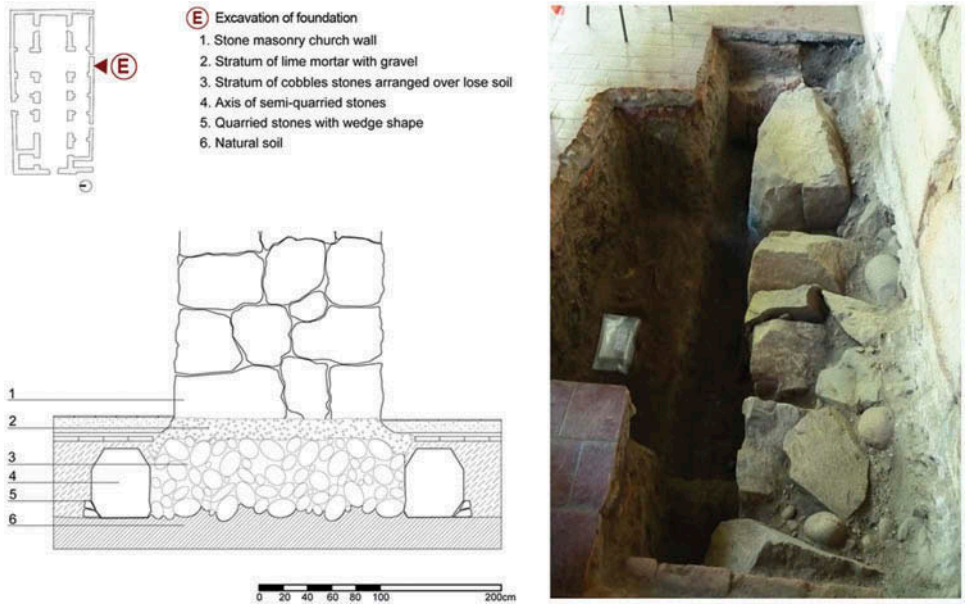

Figure 6. Section and image of the foundation of the church.

Figure 7. View of the horizontal diaphragm, both from the central nave and from the roof.

4. Mechanical proprieties of materials

The building comprises three masonry types (M01, M02, M03), according to the constructive history of the church. The Latin cross masonry walls (M01) are a cyclopean stone rubble masonry that is reminiscent of the typical Andean masonry (Figure 3c). The transverse arched walls and the perimeter walls of lateral aisles are built in brick (M02). The triangular top part of transverse walls and the top part of the central nave stone walls are in adobe (M03) (Figure 5).

To characterize the three masonries types, besides extensive visual surveys, both in situ and laboratory tests have been considered. In particular, two standard cores have been removed from stone masonry walls, and an exhaustive set of rebound tests (Controls 45-D0561 Hammer) have been carried out on stone and brick walls. Cores removal enabled to perform uniaxial compression tests on five stone samples, which have also been subjected to a petrographic analysis through observations of thin sections at the optical microscope in transmitted polarized light. Besides, mineralogical and clay minerals composition (through X ray diffraction), amount of calcium carbonate (by beans of the Dietrich Früling calcimeter) and sieve analysis for grain size distribution of mortar and adobe samples were determined.

Core samples C1 and C2 (M01 masonry type) shown in Figure 8a have been drilled from the central nave wall and the south transept wall, perforating the walls up to more than half of their thickness. Core samples revealed a masonry consisting of large white igneous stones interleaved with smaller black igneous stone elements and a little amount of mortar (Figure 8a).

The mineralogical and petrographic analysis have characterized the white rock as *Biotite Andesite* with a specific weight of 23 KN/m^3, and the black rock as

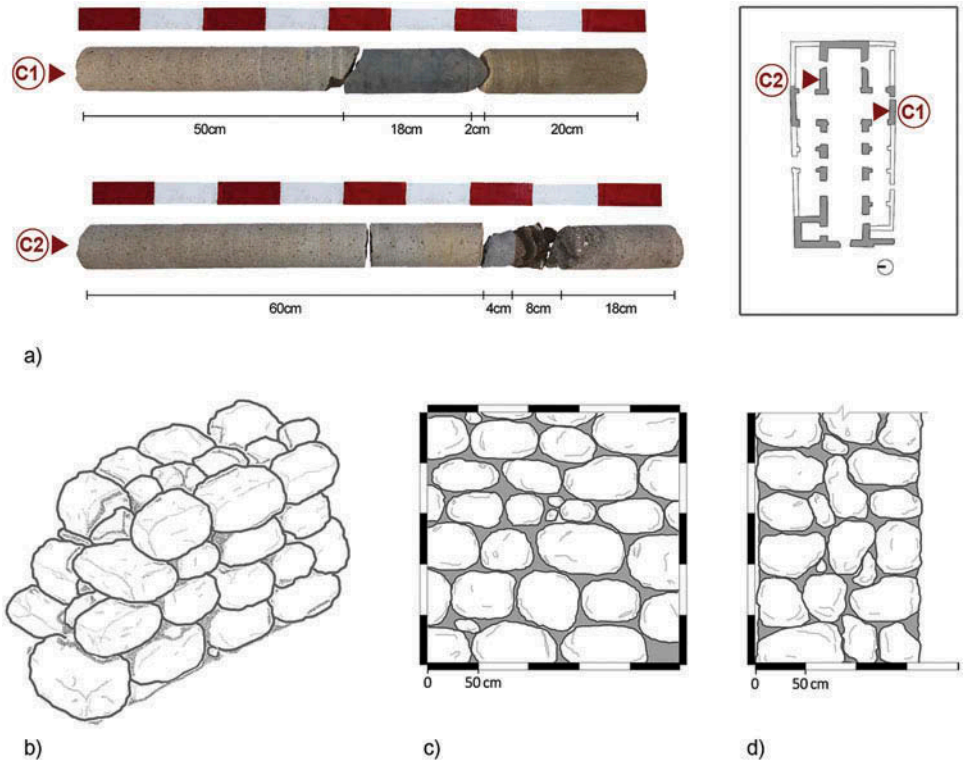

Figure 8. M01 masonry: a) coring test; b) axonometric; c) front view; and d) section.

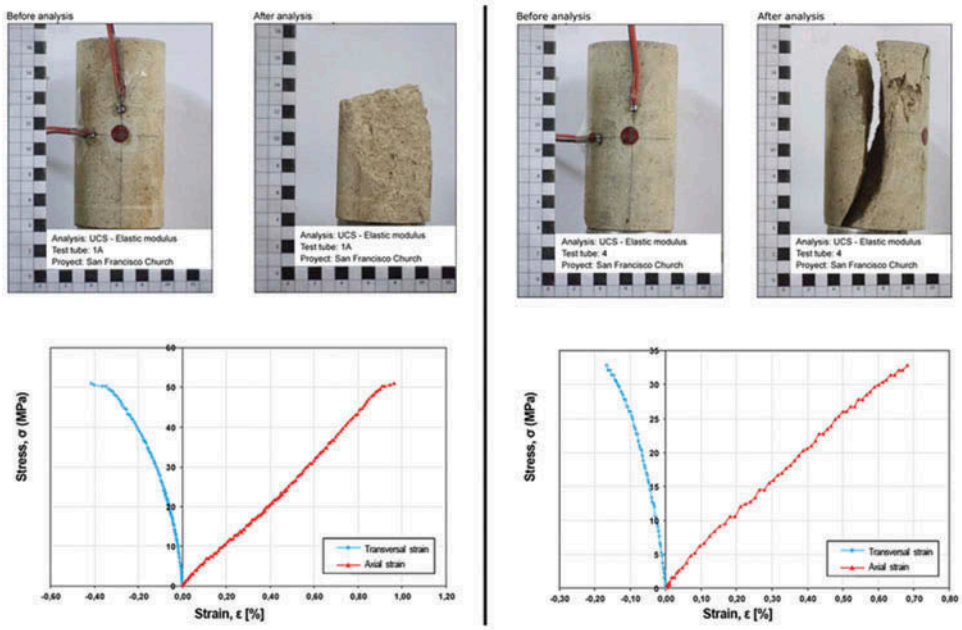

Average values of five cylindrical stone samples:	*Compressive strength* [MPa]	*Young modulus* [GPa]	*Poisson coefficient*
	47.8	5	0.26

Figure 9. Compression test on biotite samples.

Clinopyroxene Basaltic Andesite with a specific weight of 26 KN/m^3, both hypo-crystalline equigranular and isotropic rocks with different alteration. Making a comparison between this characterization of rocks from the walls and the main lithological properties of stones from different quarries in *Cerro Blanco*, the provenience of the rocks from *Cerro Blanco*, mentioned previously by historians, was confirmed.

Uniaxial compression tests were carried out on five cylindrical Biotite Andesite samples cut from cores, 74.4 mm diameter and 154 mm height, and in Figure 9 the average values of mechanical parameters are showed. In order to evaluate the compressive strength of a high number of stone blocks of M01 masonry an extensive experimental analysis by Rebound testing was carried out on stone blocks surfaces of the central nave; the deduced compressive strength of the biotite stones is 50 MPa. This indirect test determines less reliable values than the compression test: the value obtained overestimates the result of the compression test by 4.6%. Since the results of the rebound test are not dispersed (coefficient of variation 16%), it is possible to assert that the stones of M01 masonry belong to the same type.

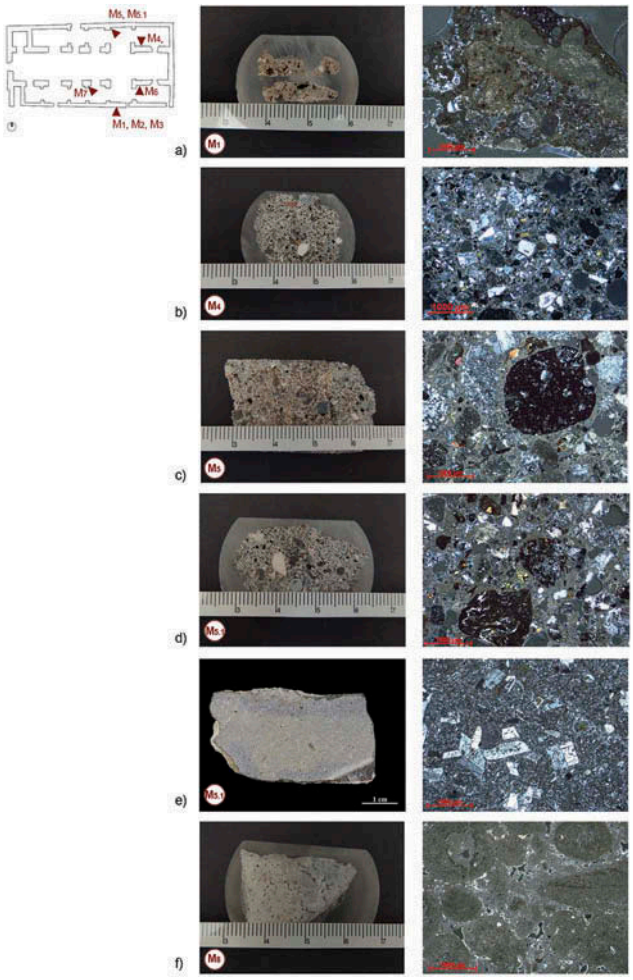

Figure 10. Thin section of joint mortar samples.

As regards mortar of the M01 masonry type, three samples—M1, M2, and M3—were collected from the south transept wall in proximity of the wall openings. Sample M4 was extracted from the first core sample C2, samples M5 and M5-1 were gathered from the northwest transept wall behind a detached tombstone and sample M8 was taken from the south wall of central nave in the space under the roof top, which probably corresponds to a surface improvement intervention.

Table 1a summarizes principal mineralogical composition, clay minerals composition of earthen portion, calcimetry, and granulometry of mortar samples, in Figure 10 thin sections of mortar samples and indication of sampling position are indicated. The mortar of samples M1, M2, and M3 seems to have been made by mixing earth and lime (1 part lime/3 parts earth). The lime is not well mixed and often shows a lumpy aspect. With respect to the aggregate grain size, the mixes are particularly lean (the main class is represented by fine sand). Such grain size composition does not guarantee high cohesion levels, which therefore must be ascribed to the addition of lime (Figure 10a). Concerning the samples M4, M5, and M5-1 they are quite similar with a scarcity of binder (Binder/Aggregate 1/3), a bimodal grain size distribution and a binder constituted by aerial lime. There is evidence of some small differences with respect to the amount of binder (sample M51 is slightly more rich in binder) and about the kind of binder (rare presence of chert fragments in samples M5 and M5-1) (Figures 10b, 10c, 10d, and 10e). A different case is the M8 sample, which is constituted by an aerial lime binder without aggregate (Figure 10f).

Extensive visual in situ surveys allowed identifying two portions of 2.5x2.5 m on central nave wall as representative of the texture of M01 masonry type. On the basis of in situ survey and of the results from the coring tests, a hypothesis of the M01 wall section could be thus defined (Figures 8b, 8c, and 8d), determining the typical dimension of *Cerro Blanco* blocks: 45–65 cm wide, 65–45 cm long, and 45 cm thick. From this wall section, an estimation of the specific weight of masonry was made: 22 KN/m^3, assuming for biotite stone 23 KN/m^3, for basalt stone 26 KN/m^3, for mortar 13.9 KN/m^3, for pebbles 20.6 KN/m^3 and evaluating a percentage of stone blocks at about 80%. Regarding masonry layout, the cyclopean stones of M01 are characterized by: an irregular but homogenous shape; search of horizontal rows; staggering of vertical joints; congruence of the stone elements size; presence of

Table 1. Principal mineralogical composition, clay minerals composition of the earthen materials, calcimetry and granulometry of mortar samples. Estimation of mechanical parameters (compressive strength, Young modulus and shear strength) obtained using Masonry Quality Index method for the masonry M01 and M02, and assumed in agreement with Chilean Standard (Instituto Nacional de Normalización—INN 2013) for the masonry M03. *calcimetry test

Mortar samples									
	Principal mineralogical composition			*Clay minerals composition*			*Granulometry*		
	Quartz %	Feldspars %	Calcite* %	kaolinite	iilite	smectite	Sand %	Silt %	Clay %
M 1	8	12	17.5	10	25	65	85.3	13.3	1.5
M 2	8	11	15.0	15	30	55	93.1	5.7	1.2
M 3	8	5	13.5	15	25	60	92.6	5.7	1.7
M 4	8	14	17.0	–	–	–	–	–	–
M 5	11	10	21.1	–	–	–	–	–	–
M 5–1	11	11	22.5	–	–	–	–	–	–
M 6	11	11	–	5	35	60	56.0	32.5	8.8
M 7	13	14	–	10	25	65	50.4	35.4	14.2
M 8	–	tr	79.4	–	–	–	–	–	–

transverse blocks that cross half of the wall thickness; all of which guarantee integrity and clamp behavior of masonry (Figures 8b, 8c, and 8d).

From the reconstruction of the wall cross section, the Masonry Quality Index (M.Q.I.) was calculated in agreement with the methodology proposed by Borri et al. (2015) and already applied and validated in Rovero et al. (2015). This method is useful when it is not possible or unreliable to carry out in situ Flat-Jack test coupled with laboratory tests and robust homogenization techniques (Feo et al. 2016). M.Q.I. indeed, allows an estimation of mechanical parameters to be obtained (compressive strength, Young modulus, and shear strength), using a qualitative description applicable to any type of wall, evaluating the agreement of the masonry features with the *rule of art*, i.e., block shape and size, horizontal rows, staggering of vertical joints, presence of transverse blocks (*diatones)*, mortar quality, and the stone strength.

The results of Masonry Quality Index for the stone masonry M01 and brick masonry M02 are showed in Table 1, together with the adobe masonry M03 data, assumed in agreement with Chilean Standard (INN 2013).

Finally, the adobe masonry M03, that characterizes the triangular top part surmounting the transverse arcades and the top part of the longitudinal walls of the nave, is built in adobes (30x60x10 cm). Two adobe samples (M6, M7) belonging to masonry type M03 have been taken and subjected to mineralogical analysis. The grain size analysis points out that they have been made with a lean earth, nevertheless richer in silt and clay minerals than the earth of samples M1, M2, M3. Considering that the clay mineral association of all these samples is similar it is possible to argue that the earthen material is the same and that for samples M1, M2, M3 raw earth was sieved removing the coarser portion.

Assessment of crack patterns

The Church of San Francisco has suffered numerous damages due to the combination of two factors: the sustained severe earthquake action and some intrinsic constructive defects inherent in the building. These structural defects are the result of some of the aforementioned transformations in the history of the building, which has given rise to structural weaknesses. Some weaknesses, both in the in-plane capacity of the walls and in the box-behavior, are basically determined by disconnections between the walls. In fact, the ability of the church to behave like a box depends on the efficiency of the connections between walls and roof, and on the adequate interlocking between orthogonal walls. Thus, although the horizontal "diaphragm" placed on the central nave has a fundamental role in the transverse seismic response it is not sufficient to mitigate the overturning of the individual walls belonging to the side aisles nor of front and rear façades.

Openings in masonry walls, and the absence of adequate connections between the additions, built with different materials, have represented the typical patterns of earthquake damage. The building, therefore, presents a complex crack pattern.

For a more efficient understanding of the severity of the damage, the crack pattern has been analyzed according to the dominant behaviour of macro-elements of churches with basilica plan (Da Porto et al. 2010; GNS Science Report 2016; Giresini 2016; Doglioni, Moretti, and Petrini 1994; Giuffrè 1991; Lagomarsino and Podestà 2004, Lagomarsino et al., 2004), considering the structural response of the building in the longitudinal and transverse directions. The considered behaviors are: the out-of-plane behavior of the façade, of behind presbytery wall and of transept walls; in-plane behavior of longitudinal nave walls and transverse arcades walls.

The in-plane behavior of the transverse arcade walls and the out-of-plane behavior of the longitudinal arcade walls have been analyzed together since these phenomena are strictly related (Figure 11). The in-plane behavior of transverse arcade walls is demonstrated by diagonal cracks in the arches and in the adobe triangular top part. This fracture pattern surely shows a strong similarity with the crack pattern characterizing the behavior of the masonry arcades under seismic action recorded in all the old churches in Santiago center (the Metropolitan Cathedral, the Agustin Church, the Merced Church, etc.), as reported by the historical sources and by the documentation of the repairs (Consejo de Monumentos Nacionales—CMN (Chile) 2010). In the current state, the behavior of transverse arcade walls is strongly conditioned by the repairs carried out in 1988, which introduced a reinforced concrete frame and upper tie-rod (Figure 4) that reduce the entity of deformations but determine a deep change of the behavior of the masonry arch. Indeed cracks due to discontinuities and lack of cohesion between masonry and concrete are visible at the intrados of arcades and in the piers. The lack of bond between the transverse arcades brick masonry and the longitudinal stone walls of the nave is evidenced by deep cracks (Figure 11a). A singular out-of-plane behavior of the longitudinal walls due to seismic actions is characterized by significant bulges in the stone-work in correspondence of the transverse arches springs (letter e) in Figure 11), probably connected to the presence of the RC tie-rod. These bulges are also associated with worryingly deep cracks and deformations in some arches piers of the nave (Figures 11b and 11c). All these phenomena are consistent with pounding effect between transverse walls and longitudinal walls, triggered by the discontinuity of the walls implemented with different building technologies, i.e., stonework and brickwork, which can hardly be bonded together. Moreover, the arches intrados in the longitudinal walls are characterized by deep cracks consequence of earthquakes actions, which indicate a separation of the wall into two leaves (Figure 11d). As regard to the bulging phenomenon of the longitudinal walls, a fundamental role can be attributed to the insertion of reinforced concrete chains in the upper part of transverse arcades walls (Figure 4 and Figure 11f). In fact, these tie-rods strongly increase the capacity against overturning but at the same time change the modalities of collapse in vertical arch mechanism connected to the bulging.

Figure 11. Transverse arcade wall: a); b); c); d) crack pattern; position of e) local bulges and f) RC-steel tie-rods.

In relation to the out-of-plane behaviors of the façade, a brick reconstruction at the gable of the façade shows a collapse occurred. The discontinuity in the thickness of the walls represents a weakness against overturning of the apex wall with a macro-element ratio Length/Height = 0.605 (D'Ayala and Speranza 2003). Moreover the discontinuities with the orthogonal walls of main nave and with external orthogonal wall of the bell tower represents an additional vulnerability associated with the eccentricity of the bell tower inducing different inertia than the main block.

In relation to the out-of-plane behavior of the rear wall of the presbytery, the reconstruction in wooden elements and brick shows a collapse that occurred at the top of the wall. These failure mechanisms are connected to the following factors: the high conventional slenderness (λ_c = 17.5) of the wall; the significant distance between the transverse walls; the ratio between length of macro-element and height on ground L/H = 0.88 (D'Ayala and Speranza 2003); the lack of a connection with the roof covering; and the presence of a wide opening.

The out-of-plane behaviors of the transepts north and south walls is apparent in the vertical fractures that indicate the constructive discontinuities between the upper parts of the transept façades and the lower part, which belongs to the original nucleus of a Latin cross (Section 1). The reconstruction in brick inserted into the original walls of stone is evidence of a previous occurred collapse.

6. Structural analysis

Safety assessment of monumental buildings requires a multi-level approach that should embrace local and global behaviors, linking causes of damage and related consequences that influence each other. Results outlined throughout Sections 3 and 4 suggest that accurate analysis has to focus on the response of those macro-elements that exhibited significant damage during past seismic events.

To this end, multiple analysis techniques have been employed. Regarding the response of those macro-elements that revealed a substantial vulnerability to out-of-plane actions, linear (LKA) and incremental kinematic (IKA) analyses addressed front façade, behind presbytery wall and transept walls, while rocking analyses focused on transepts walls. As for the in-plane response, LKA was exploited to evaluate the capacity of transverse arcade walls and FE models implemented through the commercial code DIANA constituted the basis for structural linear and nonlinear analyses.

Moreover, a control on the global response of the church has also been carried out to define preferential displacement shapes. The global response of San Francisco has been addressed through Linear Dynamic Analyses of a 3D FE model exploiting the commercial code Straus 7.

The Chilean NCh433 code does not provide the possibility to verify the seismic behavior of existing non-confined-masonry buildings, although the Chilean Standard NCh3332.Of.2013 for the Structural Intervention of Earthen Historical Buildings (Instituto Nacional de Normalización—INN 2013) provides general criteria for interventions intended to result in strengthening. For this reason, it was decided to address the gap in this standard with a combined analysis through the Italian Code NTC2008 (MIT 2008) and Circ.617/2009 (MIT 2009).

To achieve a safety estimation of the static consistency of the church, a preliminary graphical analysis for vertical loads has been first carried out on a significant portion of the main nave and transept wall through the *Safe Theorem of Limit Analysis* (Heyman 1966). An equilibrated solution has been found (drawn as a set of thrust lines) contained inside the masonry structure, compatible with the loads and which does not violate the yield conditions. This condition has guaranteed the safety of structure for vertical loads. Figure 12 shows the thrust line of each arch (1, 2, 3, and 4) with the related values of thrusts. It is worth noting that the thrust line of the transverse arcade F (Figure 12b) highlights a limit condition for the stability of portion F4, considering the thrust position at the ground. As expected from direct surveying activities, the thrust lines converging on pillar F3 are influenced by loads of both the longitudinal arcade (3) and the transverse wall facing the transept (wall F), determining a high loading level on a reduced portion of masonry which is in fact heavily damaged. Linear static analysis for vertical loads on the global 3D FEM has been carried out, and results show comparable stress levels ranging 1–1.2 MPa on portions F3 and F4.

6.1 Seismic hazard

The high level of seismicity activity in Chile is due to the contact between the Nazca Plate and the South American plate with a convergence rate ranging between 6–7 cm/yr (Khazaradze and Klotz 2003; Leyton, Ruiz, and Sepúlveda 2009). The main discussions on this issue (Barrientos 2007; Scholz 2002) all agree on the presence of two seismogenic sources that generate both shallow and deep ruptures. Shallow thrust fault events are related to interplate activity with epicenters near the coastline and with depths ranging between 15 and 50 Km. In-slab events are

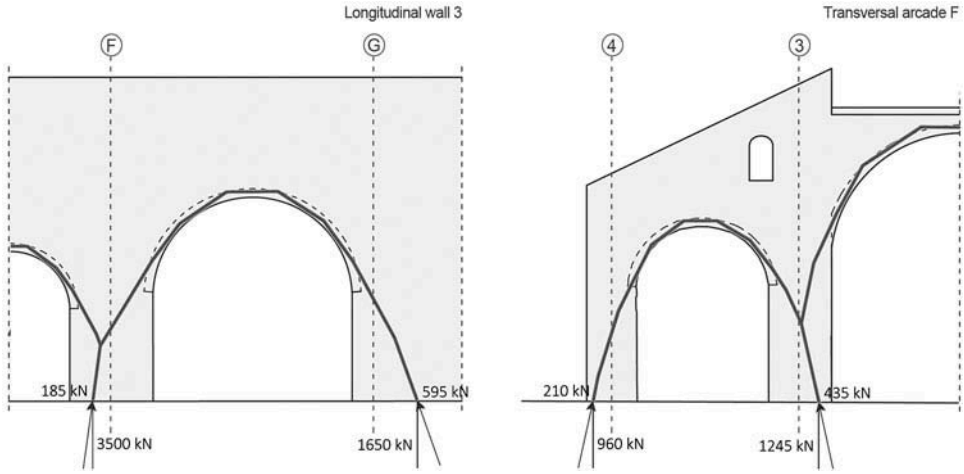

Figure 12. Thrusts line of wall portion in interception of longitudinal wall 3 and transverse arcade F (Figure 1).

instead located at depths greater than 50 Km (Kausel and Campos 1992).

In relation to the amplification effects of the Santiago basin and related crustal activity, Armijo et al. (2010) and Pérez et al. (2014) report on possible new seismic hazard scenarios for the city of Santiago in light of the activity of a newly discovered Quaternary thrust fault named San Ramon, which is placed at the foot of the West Andean fault at the eastern border of the metropolitan area. Indeed, the seismic hazard in Santiago has been mostly based until now on subduction mega-thrust earthquakes (Pérez et al. 2014).

Direct investigation on the mechanics of soil in Santiago center documented in (Vukasovic, 2013) classify the area as having very dense and stable ground (V_{S30} > 500 m/s). The newest national design regulations D.S. N° 117, (V.Y U.), DE 2010 (MINVU 2011), which partially modify the previsions of National Design Code NCh433 (INN 1996) for soil mechanics, associate a value of V_{s30}, a soil type B and a soil coefficient S = 1. In agreement with NCh433 and employing results of (Vukasovic 2013), it is possible to define an elastic spectrum, defined by the following:

$$S_e = IA_0\alpha \quad (1)$$

where I = 1.2 is the building category coefficient associated to class A constructions and A_0 = 0.3 g is the spectral acceleration determined by NCh433 (Instituto Nacional de Normalización—INN 1996). The amplification factor $\alpha = [1 + 4{,}5\ (T_n/T_0)^p]\ /[1 + (T_n/T_0)^3]$ assumes a maximum of 2.75 for $T_n = T_0$, where T_0 = 0.3 and p = 1.5 are parameters that depend on the type of soil (type soil B) evaluated according with the newest re-classification of soil factors (D.S. N ° 117, (V.Y U.), DE 2010 (Ministerio de Vivienda y Urbanismo—MINVU (Chile) 2011). It is worth underlining that soil parameters are slightly different for the Italian NTC2008 (Ministro delle Infrastrutture e dei Trasporti—MIT (Italy) 2008) and NCh433 (Instituto Nacional de Normalización—INN 1996). According to NTC2008 (Ministro delle Infrastrutture e dei Trasporti—MIT (Italy) 2008), the first vibration period of the whole church can be approximated as $T_1 = C_T H^{3/4} = 0.05 \cdot 14.12^{3/4} = 0.37$s.

Recent studies (Leyton, Ruiz, and Sepúlveda 2009, 2010) report on a third seismogenic source connected to crustal activity in central Chile, as previously outlined in Martin (1990), Algermissen (1992), Romanoff (1999), and Leyton, Ruiz, and Sepúlveda (2009), and present probabilistic re-estimation of seismic hazard and expected PGA. Even though preliminary investigations reported in (Leyton, Ruiz, and Sepúlveda 2009, 2010) require further investigation of local amplification mechanism, initial results estimate an expected peak ground accelerations equal to 0.55 g for a return period of 475 years, which is greater than that considered by the Chilean Code for the city of Santiago (zone II) A_0 = 0.3 g.

Moreover, during the Maule earthquake in 2010, which has been associated with inter-plate activity (Mw = 8.8), the Santa Lucia Hill station placed just 500 m away from San Francisco church, recorded horizontal ground accelerations in North-South direction 0.32 g and in East–West direction 0.242 g (Chilean National Seismological Centre). These values are about 30% greater than the PGA considered for the same site in the Chilean Code.

A similar earthquake also characterized by inter-plate activity is the 1985 earthquake during which the accelerograph located in Endesa building (200 m far

from San Francisco church) recorded ground accelerations peaks in N-S and E-W directions equal to 0.126 g and 0.122 g, respectively. During the most recent Illapel 2015 earthquake, the Cerro Colorado Renca station placed 3 km from the church recorded a peak in horizontal ground acceleration around 0.04 g (Chilean National Seismological Centre).

6.2 Local response models

Crack patterns on existing masonry buildings without box behavior have shown that failure is due to a loss of equilibrium and that seismic action selects the most vulnerable masonry portions whose structural response is independent of the global behavior of the building (D'Ayala 1999; Augusti, Ciampoli, and Zanobi 2002; D'Ayala and Speranza 2003; Giuffrè 1989).

An effective method to tackle such a behavior consists in applying limit analysis to macro-block models that identify rigid and fracture-separated masonry portions subjected to overturning (Lourenco 2005; Lourenco et al. 2007; Mallardo et al. 2008; Mele, De Luca, and Giordano 2003; Roca, Cervera, and Gariup 2010). This approach is first proposed in Heyman (1966) and applied to cultural heritage buildings by Giuffré (1991) and Doglioni, Moretti, and Petrini (1994), and successively exploited in many other works, such as Casapulla and D'Ayala (2006), Casarin and Modena (2008), Casolo and Sanjust (2009), D'Ayala (1999), D'Ayala and Speranza (2003), De Felice and Giannini (2001), Lagomarsino and Podestà (2004), and Lagomarsino and Resemini (2009). It has also been recently acknowledged by the Italian Seismic Code (Ministro delle Infrastrutture e dei Trasporti—MIT (Italy) 2008) and Circ.617/2009 (Ministro delle Infrastrutture e dei Trasporti—MIT (Italy) 2009).

On the other hand, exploiting dynamic analysis to control the time-dependent response of a rocking masonry macro-element has demonstrated to be an efficient tool (Abrams et al. 2017; Costa et al. 2013; Giresini, Fragiacomo, and Lourenço 2015; Giresini and Sassu 2017; Giresin et al., 2015; Lagomarsino 2015; Mauro, De Felice, and DeJong 2015; Shawa et al. 2012; Sorrentino, AlShawa, and Decanini 2011), especially when safety assessment is carried out in a probabilistic framework with an energy approach (DeJong 2012). Dynamics of the rocking block correctly describes how the stability of a masonry portion hit by an earthquake acceleration is connected to the velocity of the block rather than to its displacement capacity and, thus, instabilities derived by the well-known scale effect, (Housner 1963), can be adequately checked. This effect, indeed, cannot be thoroughly tackled either by displacement based (DBA), like IKA or by forced based approaches (FBA), although these methods are acknowledged by national seismic codes (Sorrentino et al. 2016).

Limit analysis with the kinematic approach, LKA, permits a safety assessment through the multiplier of loads, α_0, which expresses the ratio of equivalent inertial forces over vertical loads involved in the mechanism, assuming as the limit state, the first damaged state. Damage evolution and ultimate collapse, i.e., the ultimate limit state, can be considered if the capacity spectrum method is combined with limit analysis, i.e., IKA (D'ayala 2005; Doherty et al. 2002; Lagomarsino 2006).

First, mechanisms that are most likely to be activated in San Francisco have been defined for both the current state and state prior to the brick additions or RC consolidation. In fact, response to past seismic events, denoted by still visible cracks, are deeply correlated with the expected future behavior since earthquake-related damage has a progressive and relapsing character (Doglioni, Moretti, and Petrini 1994). Table 2 shows results and descriptions of the analyzed local mechanisms for the San Francisco church considering both the current state of the building and the state preceding the additions and RC insertion interventions.

The response of the transversal arcade systems in the current state is analyzed through three mechanism scenarios, TA1, TA2, and TA3, based on visible crack patterns annotated during surveying activities (Figure 13). Different scenarios represent an increasing quality of the masonry of longitudinal walls (axis 2 and 3; see Figure 1). Mechanism TA1 represents walls 2 and 3 as a two-leaf masonry, thus by means of two blocks (Figure 13a), while mechanism TA2 assumes the same masonry quality for wall 2 and 3 but a complete effectiveness of the anchoring of the piers (Figure 13b).

Table 2. Results of linear kinematic analysis of current state and of the state prior to the brick additions or concrete frame reinforcements: Kinematic multiplier α_0, Participating Mass M*, mechanism activation acceleration a_0*, Equation (2) for the demand acceleration at ground level, Equation (3) for the demand acceleration at elevated level

Masonry					
ID	*Type of masonry*	*Specific weight [KN/m3]*	*Compressive strengthfm [MPa]*	*Young modulus E [GPa]*	*Shear strength r0 [MPa]*
M01	Rubble stone masonry (Figure 8)	22	3.7	1.6	0.06
M02	Fire-brick masonry 40x22x7cm	17	3.1	1.38	0.05
M03	Adobe masonry 30x60xl0 cm	16.6	1.2	–	0.025

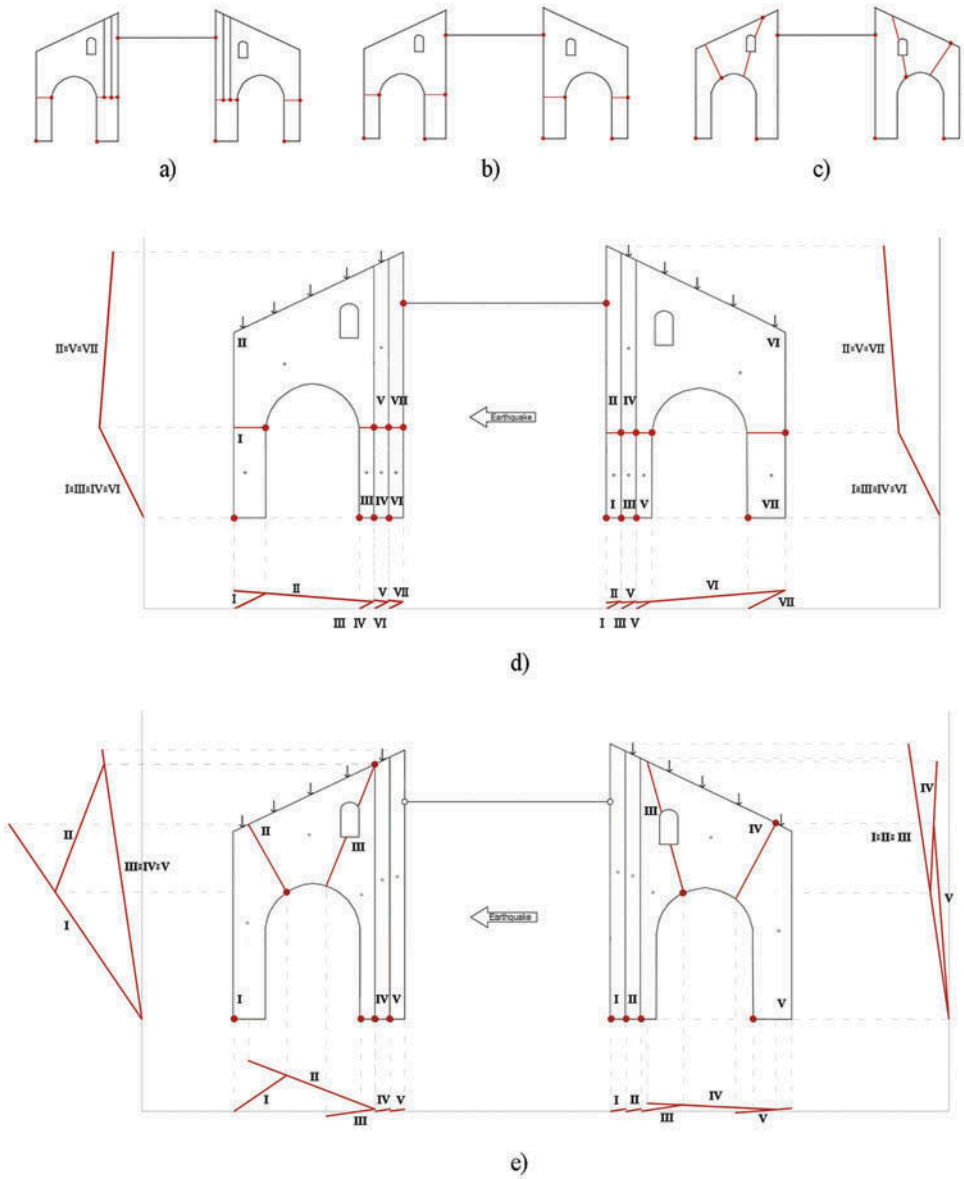

Figure 13. In-plane mechanism of the transverse arcade. Possible activated mechanisms: a) TA2 (current state) longitudinal wall made up of a two-leaf masonry and complete effectiveness of the anchoring of the piers; b) TA3 (current state) longitudinal walls as a monolithic masonry with complete effectiveness of the anchoring intervention on piers and c) TA5 (state before concrete reinforcements) longitudinal walls as a monolithic masonry. Horizontal and vertical virtual displacement diagram: d) TA1 (current state) longitudinal wall made up of two-leaf masonry and e) TA4 (state before concrete reinforcements) longitudinal wall made up of two-leaf masonry.

Mechanism TA3 (Figure 13c) represents the longitudinal walls as a monolithic masonry with full effectiveness of the anchoring intervention on piers. The hypothesized direction of the action induces a counter-clockwise mono-lateral rotation of piers and a consequent clockwise rotation of upper blocks.

Figure 14 shows the out-of-plane mechanisms identified for the current state. Mechanisms represent the overturning of gables of façade, and behind presbytery wall, i.e., MF and BP in Table 2, whose cuneiform macroblocks rock around two oblique cylindrical hinges, and the overturning of the north and south transept walls around cylindrical hinges placed 60 cm off the ground, NT and ST (Table 2).

In the state prior to the brick additions or RC consolidation the mechanisms evaluated are the same, but in different materials, with the exception of the mechanism characterizing the transverse arcades (TA4 and TA5 Table 2) and the main façade (MF1), which also have different layouts. For the in-plane mechanisms of the transverse arcade, two layouts have been considered addressing the longitudinal walls as two-leaf

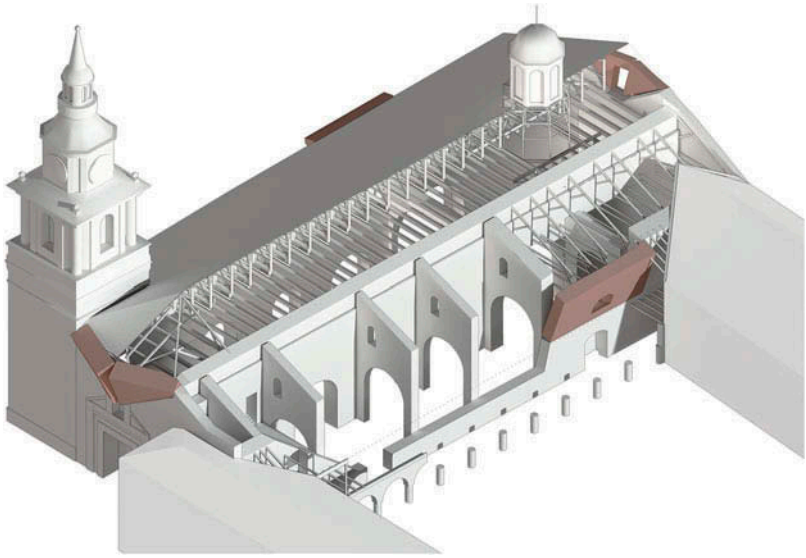

Figure 14. Local mechanisms of collapse in current state: main façade, behind presbytery wall, South and North transept walls.

masonry, TA4 Table 2 and Figure 13d, or monolithic, TA5 Table 2 and Figure 13e. The layout of both mechanisms places hinges at pier bases and on arch haunches so that a counterclockwise rotation of piers induce a clockwise rotation of the central block, which includes the keystone of the arch and the related portion of the wall above it.

In the mechanism named MF1, the gable of the main façade is considered confined by both adjacent walls and longitudinal walls, so that it becomes a horizontal bending mechanism also named the horizontal arch mechanism of confined walls (Figure 15). For this kind of mechanism the horizontal arch inside the wall reaches the limit state due to masonry crushing for compressive stress, here considered $f_{m,min}$ = 2.6 MPa, according to M.Q.I. method, (Borri et al. 2015).

After having defined mechanism layouts and characteristics, the kinematic multiplier, α_0, can be evaluated and converted into spectral acceleration a^*_0 to get a homogeneous dimension with the demand, evaluating the participating mass as a modal form of vibration:

$$a_0\left(\sum_{i=1}^{n} P_i \cdot \delta_{xi}\right) = \sum_{i=1}^{n} P_i \cdot \delta_{yi} a_0^* = \frac{a_0 \sum_{i=1}^{n+m} P_i}{M^* FC} M^* = \frac{\left(\sum_{i=1}^{n} P_i \cdot \delta_{xi}\right)^2}{g \cdot \left(\sum_{i=1}^{n} P_i \cdot \delta_{xi}^2\right)} \quad (2)$$

where α_0 is the kinematic multiplier; *Pi* is the i-th load; δxi is the virtual horizontal displacement of the gravity center of the i-th load *Pi;* δyi is the virtual vertical displacement of the gravity centers of the i-th load *Pi;* M^*_0 is the participating mass; a^*_0 is the activation acceleration; and *Fc* = 1,35 is a confidence factor related to the knowledge level of building (Ministro delle Infrastrutture e dei Trasporti—MIT (Italy) 2009; POLIMI, 2010).

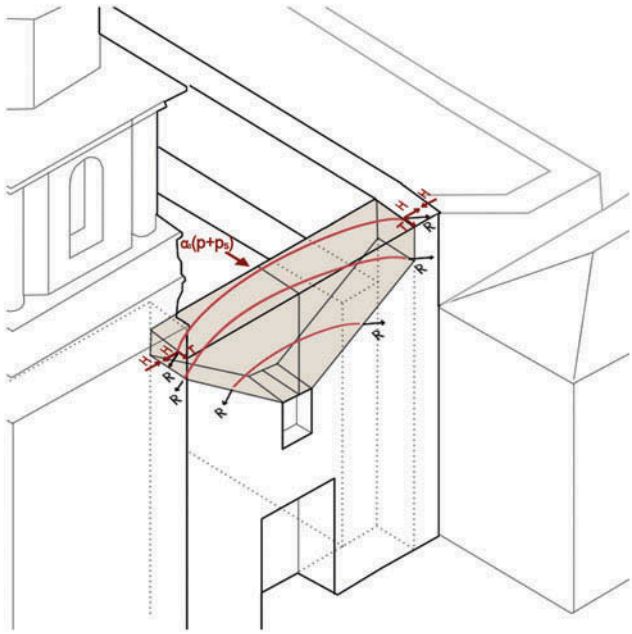

Figure 15. The horizontal arch mechanisms (horizontal bending) of the façade.

For all mechanisms, a slippage $t = 0.66 \sum_{i=1}^{n} W_i (f_d l)^{-1}$ of the cylindrical hinge is considered to take into account the finite compressive strength of the masonry and, after the onset of motion, the actual behavior of

the blocks, which present considerable thickness. Slippage t depends on i-th self-weight, W_i, design compressive strength, $f_{d=} f_m$, and width of wall, l.

Safety assessment requires that the spectral acceleration must be equal or greater than the demand acceleration, evaluated as $a_0^* \geq I\ A_0\ \alpha\ R^{*-1} = 2{,}31\ ms^{-2}$, with $R^* = 1.54$ is the acceleration reduction factor according to NCh433 (Instituto Nacional de Normalización—INN 1996) and other coefficients, as defined in Section 5.1.

Mechanisms involving the portion of masonry placed higher than ground level have an input demand amplified by the effect of height. The NTC 2008 (Ministro delle Infrastrutture e dei Trasporti—MIT (Italy) 2008) evaluates this amplification, with further verification imposing: $a_0^* \geq S_e(T_1)\Psi(Z)\gamma$. The amplification considers the design spectrum acceleration with respect to the period T_1, $S_e(T_1)$, being $T_1 = 0.05\ H^{3/4}$ the first vibration period of the macroblock. Then $\Psi(Z) = Z/H$ is a function depending on the height from the foundation of the centroid of the weight forces applied on the rigid bodies, Z, on the total height of the building from the foundation, H, and on $\gamma = 3N/(2N+1)$, which corresponds to a modal participation coefficient, depending on N number of floors.

The comparative analysis of the current state (fired-bricks blocks) and state prior to the brick additions or RC consolidation (stones blocks) shows a significant improvement of resistant behavior for the mechanisms of the transverse arcade system TA1, TA2, and TA3 and for the Main and the Presbytery Façades, MF, PF.

hese improvements, which lead to a satisfactory safety assessment for the current state, owe to a deeply different mechanism shape (arcade mechanisms and main façade mechanism) or a decrease in live loads (wooden gable on the presbytery gable). On the other hand, the walls of the north and south transepts, NT and ST, feature a worsening of the seismic behavior, due to the reduction of the resisting transverse section. Indeed, the crack pattern of transept walls, consisting of deep fractures between the transverse arcade walls (Figure 1, plan F and G) and the longitudinal walls (Figure 1, plan 1 and 4) surveyed after the 2010 earthquake, confirms the activation of the mechanism without any collapse. While for the mechanisms involving the main façade and the presbytery façade, any crack pattern has been surveyed after the 2010 earthquake when the transverse arcade systems suffered severe damage, which requires a further investigation.

In order to enrich the understanding of the local response of the transverse arcade systems and the transept walls, considering the different nature of the mechanisms analyzed, further investigations have been carried out. In particular, the mechanisms regarding the transept walls are considered through incremental kinematic analysis (IKA) and rocking analysis; and the behavior of the transverse arcades are analyzed also through structural non-linear analyses in a FEM environment.

Incremental kinematic analysis (IKA) can be applied to evaluate the decrease of the kinematic multiplier α_0 due the increase of the displacement d_k of a control point on varied geometrical configurations, repeatedly applying the principle of virtual works, assuming an increasing forcing action that cannot induce any transitory recovery of the block after the activation of motion. The displacement capacity curve obtained through IKA initiates with the value of acceleration necessary to activate the mechanism, a_0^*, and descends linearly, describing how the mechanism evolves until final failure, i.e., when the curve reaches nil value. Results of IKA can be used on properly damped response spectra but does not constitute an alternative to estimations offered by a nonlinear dynamic.

Real out of plane mechanisms NT and ST are thus transformed into equivalent SDOF systems, whose capacity in displacement have to be compared with the related Acceleration Displacement Response Spectrum (ADRS), as shown in Figure 15.

The finite rotation value $\theta_{k,0}$ that leads a macroblock to collapse is connected with the zeroing of the stabilizing moment, $M_s = P_i\ R_i\ Cos(\beta_i + \theta_{k,0}) = 0$. The expression of the stabilizing moment takes into account the i-th force, P_i, the distance between the i-th point of force application and the pivoting hinge, R_i, and is the angle comprised by the horizontal and R_i, named β_i. Thus the horizontal displacement of the control point at collapse is $d_{k,0} = H_{cp}\ /Sin(\theta_{k,0})$.

Transforming the real system in an equivalent SDOF system, the spectral displacements of the control point at collapse is $d^*_0 = d_{k,0}\ \{(\Sigma P_i \delta^2_{xi})/[\delta^2_{x,k}(\Sigma P_i \delta_{xi})]\}$, where $\delta_{x,k}$ and δ_{xi} are the horizontal virtual displacement of the control point and the i-th force respectively. The safety condition is a displacement demand, Δ_d, lower than the ultimate displacement capacity, d^*_u:

$$d^*_u \Delta_d \tag{3}$$

where

$\Delta_d = \max\ \{S_{De}(T_s);\ S_{De}(T_1)\Psi(Z)\gamma\{(T_s/T_1)^2/[(1- T_s/T_1)^2 + 0{,}02(T_s/T_1)]^{o,5}\}\ \}$; $T_s = 2\pi\ (d_s^*/a_s^*)^{o5}$; $d^*_s = 0{,}4\ d_u^*$; $a^*_s = a_0^*(1- d_s^*/d_0^*)$ and $d^*_u = 0{,}4\ d_0^*$

From the comparison between the displacement Capacity and Demand (3) of both the transept walls, the tests are satisfied (Figure 16). Despite the activation

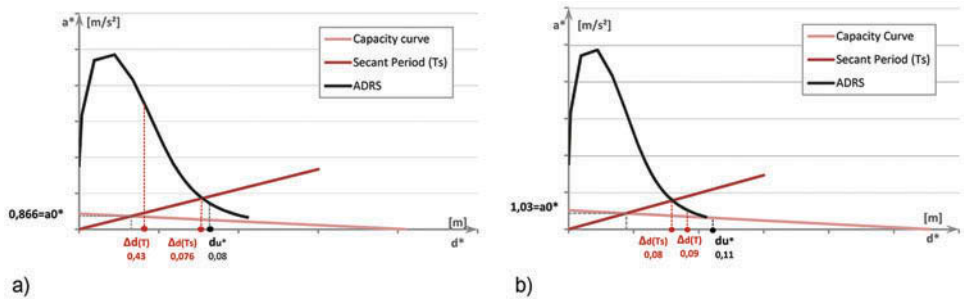

Figure 16. Capacity and demand curves of incremental kinematic analysis: a) North transept and b) South transept walls.

of the mechanisms, both macro-elements (NT and ST) show a satisfactory capacity in displacement, which justifies the absence of the collapse.

Safety estimations offered by IKA are inherently comparable to outcomes of rocking analysis, which considers the dynamic out-of-plane response of macro-elements. Give the vast literature on the issue, only basic references on the rocking block are here reported (Yim et al. 1980; Hogan 1989; Housner 1963; Makris and Roussos 2000; Makris and Konstantinidis, 2003; Shenton 1996). Relevant and recent conclusions on the opportunity and the effectiveness of representing the out of plane behavior of masonry portions as rocking blocks subjected to

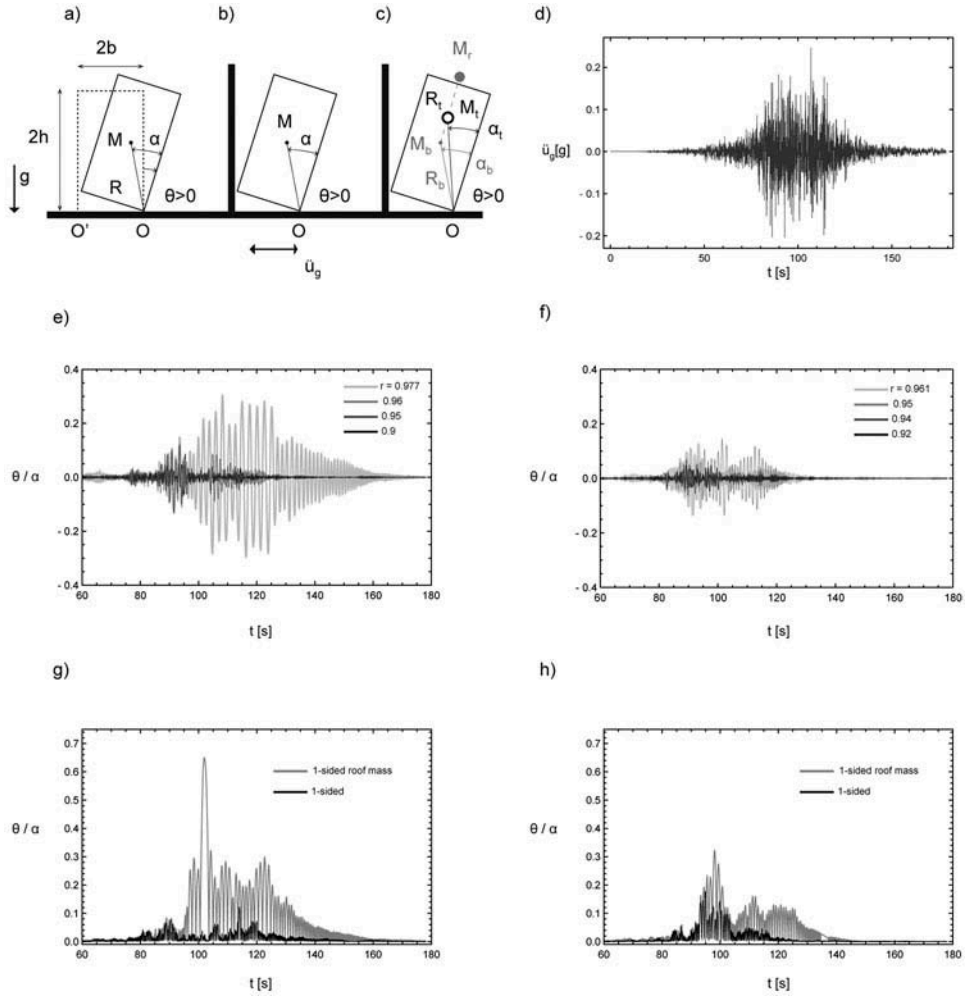

Figure 17. Considered rocking models: a) two-sided; b) one-sided; c) one-sided with overburden load on mid top. Rocking analysis: d) acceleration time history of the 2010 shake; rotation time histories for two sided rocking for decreasing values of coefficient of restitution for e) north and f) south transept walls; and rotation time histories for one sided rocking (black) and one-sided rocking with overburden weight on mid top (grey) for g) north and h) south transept walls.

strong-motions can be found in (Abrams et al. 2017; Mauro, De Felice, and DeJong 2015; Lagomarsino 2015; Shawa et al. 2012; Lagomarsino 2015; Sorrentino, AlShawa, and Decanini 2011; Sorrentino et al. 2016). Rocking analysis permits the evaluation of rotation response for an acceleration input by means of numerical integration of equation of motion derived from Lagrange's principle. Given a masonry block defined by dimensions reported in Figure 17a, which start pivoting on corner O, the compact form of the governing ODE is:

$$\begin{aligned} &I_0\,\ddot{\theta}(t) + M\,gR\sin[\alpha \mathrm{sgn}[\theta(t)] - \theta(t)] \\ &\quad = -M\,\ddot{\theta}_g(t)R\cos[\alpha \mathrm{sgn}[\theta(t)] - \theta(t)] \end{aligned} \tag{4}$$

where sgn[θ(t)], the sign function, takes into account the inversion in the rotation sign when the block reaches the ground and start pivoting on opposite corner, O' (Figure 17a). At impact moment, it is assumed that rotation continues smoothly and that angular velocity before impact, $\dot{\theta}_1(t_i^-)$, experiences a sudden decrease after impact, $\dot{\theta}_2(t_i^+)$, evaluated through the coefficient of restitution, r = 1–3/2 $\mathrm{Sin}^2[\alpha]$ for a rectangular block, imposing conservation of moment of momentum with respect to the forthcoming pivot point, O', before and after impact. Coefficient of restitution, which ranges between 0 and 1 for, respectively, perfectly plastic and elastic impacts, can be treated as an independent parameter, given the extreme sensitivity of the response to its value.

Angular velocity after impact, $\dot{\theta}_2(t_i^+) = \pm r\dot{\theta}_1(t_i^-)$, becomes one of the two initial conditions to be considered for integration after impact. The restitution coefficient has a minus sign when the one-side rocking is considered (Figure 17b). In this case, Equation (4) takes only positive values of rotation.

If the masonry block considered bears any load transferred by a roof, the contribution is considered as a concentrated mass, M_r, placed on top of the block, i.e., at R_r and α_r, transmitting dead and inertial loads, Figure 17c, and equation of motion takes the following form (Mauro, De Felice, and DeJong 2015):

$$\begin{aligned} &\left(I_0 + M_r R_r^2\right)\ddot{\theta}(t) + M_t g R_t \sin[\alpha_t - \theta(t)] \\ &\quad = -M_t \ddot{u}_g(t) R_t \cos[\alpha_t - \theta(t)] \end{aligned} \tag{5}$$

where M_t is total mass consider at the center of gravity of the whole system, identified by R_t and α_t.

Blocks representing the portions walls of north and south transept (geometrical and dynamic characteristics reported in Table 2) have been subjected to the record of the seismic event on 2010 from Santa Lucia station (Figure 17d), placed few hundred meters far from San Francisco church.

The response of transept mechanisms is showed for two-sided mechanisms (Figures 17e and 17f), for decreasing values of coefficient of restitution assuming an undamaged configuration block edges (Sorrentino et al. 2008). For one-sided rocking and for one-sided rocking considering the mass of the roof on top of the block the highest value of the coefficient of restitution has been assumed (Figures 17g and 17h).

Given the crack pattern reported in previous sections and the absence of restraining devices, e.g., tie rods or proper interlocking between transept façade and transverse walls, any added stiffness contrasting or delaying pure rocking have been modeled.

Numerical integrations have been carried out in a Wolfram Mathematica environment choosing the Gear BDF method (Gear 1971) with maximum step size 1e-4, relative error 1e-8 and an event locator to detect automatically impact instant.

To understand fully the in-plane response of the transverse arcades of the church and the difference in the response due to the RC insertions, nonlinear analyses on 2D FEM models in a TNO DIANA environment (DIANA 10. 2016) have been carried out and the response in the unreinforced has been compared to that the reinforced configuration, as after the 1988 interventions.

Referring to the worst loading configuration, models represent the transverse arcade crossing the first arch of the north nave and the second arch of the south nave (Figure 18). The mesh represents the brickwork masonry (M02) walls of the arcades of lateral naves, on which portions of adobe masonry (M03) walls rest and the cross sections of the stone masonry (M01) of the longitudinal walls facing the central nave. The restraining action of the wooden roof is represented by two rigid crossing links, which ensure the coupling of the two portions, (not plotted in Figure 18).

The 2D models are both constituted by plane strain elements named CQ16E (eight-node quadrilateral isoparametric) and CT12E (six-node triangular isoparametric) both based on quadratic interpolation and area integration. The choice of plane strain elements is due to: first, the relevant thickness of the transverse arcade, which would require too coarse a mesh of plane stress elements; and, second, the worthlessness of the out of plane response, at least weakly restrained by the planar configuration, in comparison with the in-plane vulnerability. Loads transferred from the roof to the walls are applied in five groups of point forces corresponding to the support area of secondary roof beams.

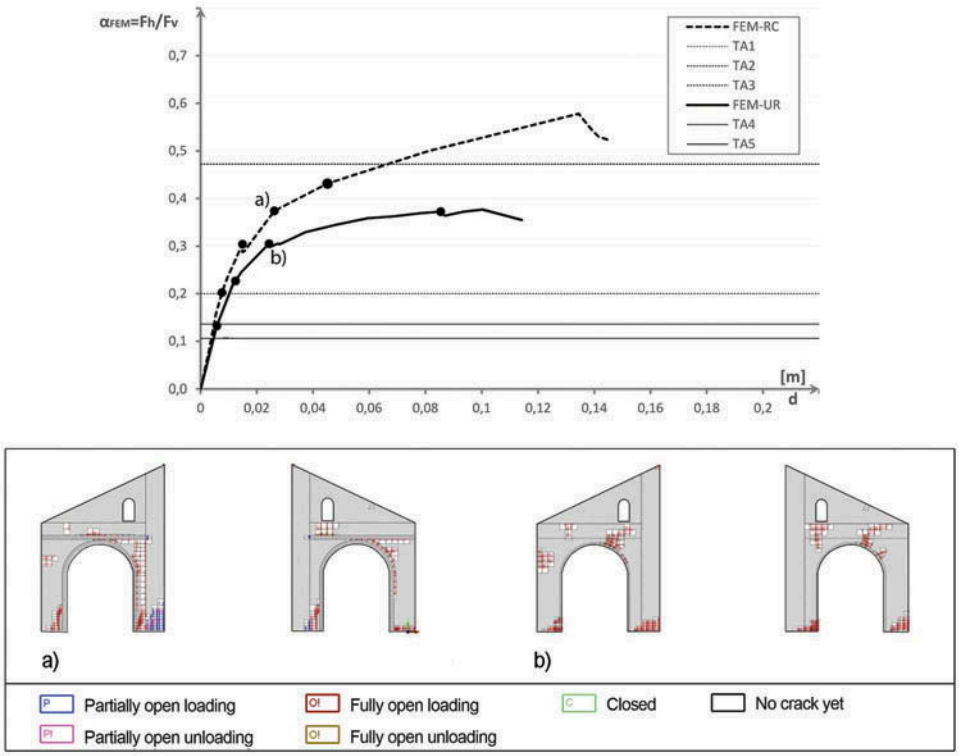

Figure 18. Structural nonlinear FEM output: curves load factor over lateral displacement and corresponding crack status for model representing the current state at load factor equal to a) 0.374; and for the state prior to the brick reconstructions or concrete reinforcements at load factor equal to b) 0.305.

After undertaking linear static analyses for vertical loads, modal and frequency response analyses permitted the definition of the displacement shape of the first vibration mode and related frequencies. Consequently, force profiles proportional to first vibration mode constituted the load set to be incremented during structural nonlinear analyses.

The insertion of RC beams in the transverse section, as expected, influences both the displacement shape and the first eigenfrequency, clearly the only relevant. In particular, the unreinforced model shows a first eigenfrequency equal to 3.47 Hz (81% x-direction participating factor), while for the reinforced model is 4.48 Hz (79.6% x-direction participating factor). Accordingly, the starting base shear for the reinforced model is 88% higher than the UR model (4.18 KN vs. 7.86 KN).

Physical non-linearities are assigned only to elements representing stone masonry (M01) and brickwork masonry (M02), due to the relevantly lower elasticity of adobe brick masonry (M03). In particular, a Mohr-Coulomb plasticity model is associated with a total strain crack model with brittle tension softening and multilinear compression softening. The brittle constitutive model for tension behavior is chosen because of the absence of in situ tests on non-linear behavior (e.g., double flat-jack or double shear tests). Moreover, especially for masonry M01, the block-dependent behavior is dominant such that a sudden loss of bearing capacity is expected (Giamundo et al. 2014).

The introduction of RC frames and tie-rods in the transverse arcade during 1988 interventions altered, although not drastically, both mass and the stiffness of the wall with respect to the unreinforced configuration, resulting in a different base shear. For this reason, shear values reported in pushover curves have been normalized to the related vertical weight. In so doing, a direct comparison with estimations offered by kinematic analysis is possible.

Figure 18 compares curves load factor over lateral displacements of centers of gravity of the UR and Reinforced models, with outputs from kinematic analyses of the correspondent mechanisms. Circle pointers show load step as reported for the reinforced configuration in Figures 18a and in the unreinforced configuration in Figures 18b. A good agreement is found between the results of the two analyses.

6.3 Global response model

In addition to the local analysis, FE models of the Church have been developed by using the software

Table 3. Natural frequencies analysis output: first 10 vibration modes

State	ID	Block	Mechanism Type	α_o	M* [kN]	a_o* [m/s^2]	$(IA_0a)/R$*	$S_a(T_1)\Psi(z)y$	R [m]	α [rad]	r	p [s-1]	Mr/Mb
Current State	TA1	Transversal	In-plane	0.473	1068	3.68	2.31	2.22	4.055	0.123	0.977	1.347	0.134
	TA2	Arches 1	behavior	0.2	1054	1.57	2.31	2.34	3.674	0.164	0.960	1.415	0.095
	TA3	Transversal	In-plane	0.472	1093	3.59	2 .31	1.01					
	BP	Arches 2	behavior	0.286	60	2.468	2.31	2.16					
	MF	Transversal	In-plane	0.336	122	2.478	2.31						
	NT	Arches 2	behavior	0.113	172	0.866	2.31						
	ST	Behind	Gable	0.131	188	1.030	2.31						
		Presbytery wall	Overturning										
		Main Facade	Gable										
			Overturning										
		North Transept	Simple										
			Overturning										
		South Transept	Simple										
			Overturning										
State prior to the brick additions or concrete	TA3	Transversal Arches1	In-plane behavior	0.106	717	1.59	2.31	-					
	TA4	Transversal Arches2	In-plane behavior	0.136	755	1.17	2.31	-					
	BP1	Behind	Gable	0.222	103	1.71	2.31	2.22					
		Presbytery wall	Overturning										
framework reinforcements	MF1	Main Facade	Horizontal arch	0.271	156	2.06	2.31	2.34					
	NT1	North Transept	Simple Overturning	0.141	334	1.063	2.31	1.01					
	ST1	South Transept	Simple Overturning	0.166	303	1.282	2.31	2.16					

Mode	Frequency (Hz)	Modal Mass	PX-X%	PX-Y%	BX-Z%
1	3.21	9.39E+05	5.69	21.43	0.05
2	3.76	8.30E+05	10.13	12.81	0
3	4.30	2.36E+06	0.06	30.64	0.01
4	6.13	2.06E+06	1.92	0.05	0
5	6.62	1.30E+05	22	0.043	0.083
6	7.03	3.62E+02	0.226	0.00	0.001
7	7.17	2.55E+04	14	0.427	0.056
8	7.42	1.07E+06	5	7	0
9	7.69	6.51E+05	1	0.042	0.692
10	8.16	1.96E+05	6	2	0.08

Straus 7 (Strand 2004). The global structure was modeled considering homogeneous and elastic materials characterized by the mechanical proprieties as reported in Section 3. As for decorative elements, they are not included in the model, and the bell tower top and the non-structural loads of roof have applied as vertical forces. A linear static analysis for vertical loads was performed followed by a natural frequencies analysis for setting the spectral response. All loading configurations have been combined to evaluate the stress and displacement. In agreement with the NCh433Of96 (Instituto Nacional de Normalización—INN 1996) the analysis included all the modes (100 vibration modes) necessary so that the sum of the equivalent masses, for each of the seismic action, is higher than 90% of the total mass. In Table 3 relevant information for the first ten vibration modes are reported since they excite most of the 90% of the participating mass.

Displacement shapes and mass distribution among different vibration modes resulting from the linear dynamic analysis are completely coherent with assumptions made for local response behavior (e.g., shapes of macroelelements) through linear kinematic analysis, even though linear elastic FEA may present significant limitations for any further investigation on masonry material. In particular, the first vibration frequency evaluated through FEM is 3.21Hz and has a participating mass factor under 25%. Moreover, in the first ten vibration modes reported in Table 3 the participating mass is just 74% in y-direction and 64% in x-direction. In fact, the distribution of the effective masse is not prevalent in a single mode of vibration but is dispersed in numerous modes. This circumstance allows asserting that the structure does not exhibit a well-defined global behavior and that the evaluations based on local analysis are more significant. More specifically, the displaced configurations for modes 3 and 7 (Figure 19) underline the intrinsic vulnerability and the related possible crack patterns of transept walls, transversal arcade systems and gables of main and presbytery facades.

7. Conclusions

This study presented the results of investigations based on a multidisciplinary approach that exploited

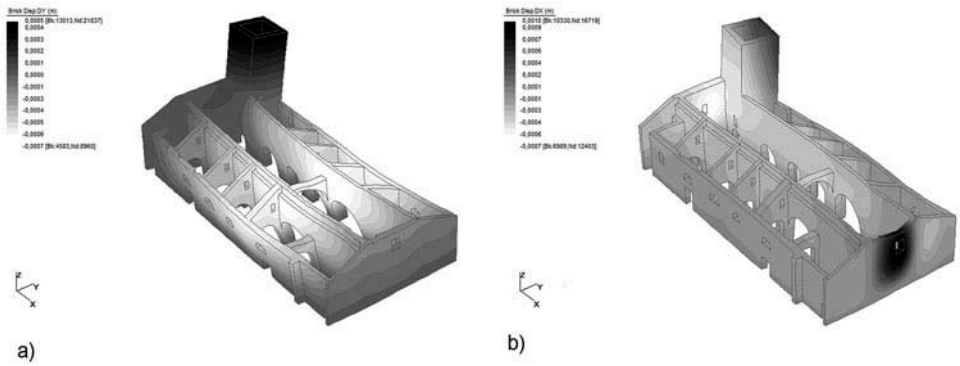

Figure 19. Linear dynamic FEM analysis output: displacement mode3 and mode7.

historical researches, direct surveys on building techniques and crack pattern, in situ and laboratory testing and multilevel structural analysis.

The study showed the relationship between the San Francisco church and the original Andean churches according to the striking similarity of architectural features and the cyclopic stonework of walls and their implementation technique. In addition, evidence of direct connections with pre-Columbian building technology, traditionally and inherently anti-seismic, appeared evident during excavations along foundation walls.

The study allowed the identification of key factors that prevented the collapse of the monument, although recurrent damages caused by strong earthquakes occurred:

- suitable size ratios of structural and architectural elements;
- the efficient constructive technique;
- the efficient transverse connection provided by the wooden beam;
- the addition of side aisles, operating as buttresses for the original Latin cross plan and use of triangular buttresses in the extrados of the arcades to ensure a better transverse response; and
- uninterrupted use and maintenance work.

Nevertheless, the high frequency of strong earthquakes over centuries caused recurrent and significant damage patterns and this investigation has highlighted main critical points.

Local-level evaluations have provided a robust assessment of the out-of-plane behavior of front and rear gables and of upper parts of transept walls suggesting that vulnerability could be successfully reduced through light interventions. Indeed, results of LKA for the overturning of the gables offered a satisfactory safety assessment considering the blocks as if they were resting at ground level, while assuming their actual position returns a negative assessment. However, neither front gable nor gable of the wall behind presbytery suffered from any damage during the strong shake in 2010. For mechanisms of north and south transept walls, LKA offered an unsatisfactory safety assessment, safety index 0.375 for north transept and 0.445 for south transept, while IKA provided a safety index equal to 1.86 and 1.375 for north and south transept respectively. Rocking analysis showed indeed that rotations reached by transept walls for the strong motion of 2010 are far away from instability even when the roof mass transmitted on top of walls is considered.

Regarding in-plane capacity, the main vulnerability is connected to the transverse response of the church. In fact, the presence of the transverse arcades undoubtedly has reduced the out-of-plane response of longitudinal nave walls and improved its stiffness, reducing the effective length to a single span. However, the lacking connection between longitudinal nave wall and transverse arcade, first, reduced the retaining effect and, second, possibly eased a pounding effect amplifying the response of longitudinal wall and inducing vertical cracks of piers.

Limit analysis and FE non-linear static analysis highlighted this weakness and the necessity of improving the lacking connections and the capacity of stone piers, given the severe load concentration levels clarified by thrust-line graphical analysis.

Moreover, through FE non-linear static analysis, an evaluation of the contribution of the reinforced concrete insertion in the arcades after 1985 earthquake was possible. Results showed that inserting RC-steel tie-rod guaranteed lower displacement levels in the arcades. Nonetheless, RC frames changed the natural behavior of masonry arches and overall transverse wall, actually transforming them into a “hybrid” structural system. In addition, the increased stiffness of this mixed RC-

masonry portion clearly enhanced damage levels on longitudinal walls, in particular at abutment level and on the piers.

Lastly, global-level evaluations confirmed the prominent by-part response of the church. Indeed, results of modal analysis demonstrated that mass participating to the first eigenmode is less than 25% and that any of the first ten modes do not excite more than 30% of the mass in a single direction. Thus, the structure does not exhibit a preferential global behavior, and it is better interpreted through local analyses, which enforce and suggest simple and straightforward intervention strategies.

Acknowledgments

The authors thank the contribution of Sara Stefanini undertaking a Master degree at Architectural Department of the University of Florence on the San Francisco Church.

Funding

The authors thank the Chilean NATIONAL COMMISSION FOR SCIENTIFIC & TECHNOLOGICAL RESEARCH-FONDECYT for funding the research project 'Initiation into Research 2013 number 11130628'.

References

Consejo de Monumentos Nacionales – CMN (Chile). 2010. *Catastro Sismo 27 de Febrero 2010, VII Región del Maule, Informe Preliminar al 19 de Marzo*. Santiago, Chile: Consejo de Monumentos Nacionales.

Abrams, D. P., O. AlShawa, P. B. Lourenço, and L. Sorrentino. 2017. out-of-plane seismic response of unreinforced masonry walls: Conceptual discussion, research needs, and modeling issues. *International Journal of Architectural Heritage* 11 (1):22–30.

Algermissen, S. T., E. Kausel, S. Hauson, and P. C. Thenhaus. 1992. Earthquake hazard in Chile. *Revista Geofísica* 37: 195–218.

Armijo, R., R. Rauld, R. Thiele, G. Vargas, J. Campos, R. Lacassin, and E. Kausel. 2010. The West Andean Thrust, the San Ramon's Fault, and the seismic hazard for Santiago, Chile. *Tectonics* 29 (2):1–34.

Astroza, M., F. Cabezas, M. Moroni, L. Massone, S. Ruiz, E. Parra, F. Cordero, and A. Mottadelli. 2010. *Intensidades sísmicas en el área de Daños del Terremoto del 27 de Febrero de 2010*. Santiago, Chile: Departamento de Ingeniería Civil, Universidad de Chile. http://eqclearinghouse.org/co/20100227-chile/wp-content/uploads/2010/04/Informe-de-Intensidades-M.-Astroza-y-otros.pdf (accessed July 13, 2017).

Atkinson, G., and D. Wald. 2007. Modified Mercalli Intensity: A surprisingly good measure of ground motion. *Seism Researcher L* 78:362–68. doi:10.1785/gssrl.78.3.362.

Augusti, G., M. Ciampoli, and S. Zanobi. 2002. Bounds to the Probability of Collapse of Monumental Buildings. *Structural Safety, Elsevier* 24 (2):89–105. doi:10.1016/S0167-4730(02)00019-X.

Barrientos, S. 2007. Earthquakes in Chile. In *The Geology of Chile*, edited by T. Moreno, and W. Gibbons, 263–87. London, UK: Geological Society.

Benavides, A. 1988[1941]. *La arquitectura en el virreinato del Perú y en la capitanía general de Chile*. Santiago, Chile: Andrés Bello.

Benavides, J., R. Márquez De La Plata, and L. Rodríguez. 1977. *Arquitectura del altiplano. Caseríos y villorrios ariqueños*. Santiago, Chile: Facultad de Arquitectura y Urbanismo Universidad de Chile.

Borri, A., M. Corradi, G. Castori, and A. De Maria. 2015. A method for the analysis and classification of historic masonry. *Bulletin of Earthquake Engineering* 13 (9):2647–65. doi:10.1007/s10518-015-9731-4.

Casapulla, C., and D. D'Ayala. 2006. In-plane collapse behavior of masonry walls with frictional resistances and openings. In *Proceedings of 5th international conference SAHC06*, edited by P. B. Lourenço, P. Roca, C. Modena, and S. Agrawal, Vol. 2, 1159–66. New Delhi, India: Macmillan India Ltd.

Casarin, F., and C. Modena. 2008. Seismic assessment of complex historical buildings: Application to Reggio Emilia cathedral. *International Journal of Architectural Heritage* 2 (3):304–27. doi:10.1080/15583050802063659.

Casolo, S., and C. Sanjust. 2009. Seismic analysis and strengthening design of a masonry monument by a rigid body spring model: The "Maniace Castle" of Syracuse. *Engineering Structures* 31 (7):1447–59. doi:10.1016/j.engstruct.2009.02.030.

Costa, A. A., A. Arêde, A. Penna, and A. Costa. 2013. Free rocking response of a regular stone masonry wall with equivalent block approach: Experimental and analytical evaluation. *Earthquake Engineering & Structural Dynamics* 42 (15):2297–319. doi:10.1002/eqe.2327.

D'ayala, D. 2005. force and displacement based vulnerability assessment for traditional buildings. *Bulletin of Earthquake Engineering* 3 (3):235–65. doi:10.1007/s10518-005-1239-x.

D'Ayala, D. 1999. Correlation of seismic vulnerability and damage between classes of buildings: Churches and houses. In *Seismic damage to masonry buildings*, edited by A. Bernardini, 41–58. Rotterdam, Netherlands: Balkema.

D'Ayala, D., and E. Speranza. 2003. Definition of collapse mechanisms and seismic vulnerability of historic masonry buildings. *Earthquake Spectra* 19 (3):479–509. doi:10.1193/1.1599896.

Da Porto, F., B. Quelhas Da Silva, F. Lorenzoni, P. Girardella, and M. R. Valluzzi. 2010. New integrated knowledge based approaches to the protection of cultural heritage from earthquake-induced risk. In *4th structural engineers world congress*. Italy: At Villa Erba, Como, Italy.

De Felice, G., and R. Giannini. 2001. Out-of-plane seismic resistance of masonry walls. *Journal of Earthquake Engineering, Taylor and Francis* 5 (5):253–71. doi:10.1080/13632460109350394.

De Ramón, A. 2000. *Santiago de Chile (1541-1991). Historia de una sociedad urbana*. Santiago, Chile: editorial Sudamericana.

DeJong, M. J. 2012. Amplification of rocking due to horizontal ground motion. *Earthquake Spectra* 28 (4):1405–21. doi:10.1193/1.4000085.

DIANA 10. 2016. *DIANA 10: User's guide*. Delft, Netherlands: TNO Building and Construction Research.

Doglioni, F., A. Moretti, and V. Petrini. 1994. *Le chiese e il terremoto: Dalla vulnerabilità constatata nel terremoto del Friuli al miglioramento antisismico nel restauro, verso una politica di prevenzione*. Trieste, Italy: Lint Editoriale.

Doherty, K., M. Griffith, N. Lam, and J. Wilson. 2002. Displacement-based seismic analysis for out-of-plane bending of unreinforced masonry walls. *Earthquake Engineering and Structural Dynamics* 31 (4):833–50. doi:10.1002/eqe.126.

Feo, L., R. Luciano, G. Misseri, and L. Rovero. 2016. Irregular stone masonries: Analysis and strengthening with glass fibre reinforced composites. *Composites Part B: Engineering* 92:84–93. doi:10.1016/j.compositesb.2016.02.038.

Fratini, F., E. Pecchioni, L. Rovero, and U. Tonietti. 2011. The earth in the architecture of the historical centre of Lamezia Terme (Italy): Characterization for restoration. *Applied Clay Science* 53 (3):509–16. doi:10.1016/j.clay.2010.11.007.

Gamrani, N., K. R. Chaham, M. Ibnoussina, F. Fratini, L. Rovero, U. Tonietti, M. Mansori, L. Daoudi, C. Favotto, and N. Youbi. 2012. The particular "rammed earth" of the Saadian sugar refinery of Chichaoua (XVIth century, Morocco): Mineralogical, chemical and mechanical characteristics. *Environmental Earth Sciences* 66 (1):129–40. doi:10.1007/s12665-011-1214-6.

Gazeta Ministerial de Chile 1822-1823 III. 1966. *Documentos relativos a los efectos del terremoto del día 19 de noviembre*. Santiago, Chile.

Gear, C. W. 1971. The automatic integration of ordinary differential equations. *Communications of the ACM* 14 (3):176–79. doi:10.1145/362566.362571.

Giamundo, V., V. Sarhosis, G. Lignola, T. Sheng, and G. Manfredi. 2014. Evaluation of different computational modelling strategies for the analysis of low strength masonry structures. *Engineering Structures, Elsevier* 73:160–69. doi:10.1016/j.engstruct.2014.05.007.

Giresini, L. 2016. Energy-based method for identifying vulnerable macro-elements in historic masonry churches. *Bulletin of Earthquake Engineering* 14 (3):919–42. doi:10.1007/s10518-015-9854-7.

Giresini, L., M. Fragiacomo, and P. B. Lourenço. 2015. Comparison between rocking analysis and kinematic analysis for the dynamic out-of-plane behavior of masonry walls. *Earthquake Engineering & Structural Dynamics* 44 (13):2359–76. doi:10.1002/eqe.2592.

Giresini, L., and M. Sassu. 2017. Horizontally restrained rocking blocks: Evaluation of the role of boundary conditions with static and dynamic approaches. *Bulletin of Earthquake Engineering* 15 (1):385–410. doi:10.1007/s10518-016-9967-7.

Giuffrè, A. 1989. *La meccanica nell'architettura: La statica*. Rome, Italy: La Nuova Italia Scientifica.

Giuffrè, A. 1991. *Lettura sulla meccanica delle murature storiche*. Rome, Italy: Kappa.

Gross, P. 2015. *Arquitectura en Chile. Desde la prehispanidad al centenario*. Santiago, Chile: Editorial Sa Cabana.

Heyman, J. 1966. The Stone skeleton. *International Journal of Solids and Structures* 2 (2):249–79. doi:10.1016/0020-7683(66)90018-7.

Hogan, S. 1989. On the dynamics of rigid-block motion under harmonic forcing. *Proceedings of the Royal Society of London A: Mathematical, Physical and Engineering Sciences* 425:441–76. doi:10.1098/rspa.1989.0114.

Housner, G. W. 1963. The behavior of inverted pendulum structures during earthquakes. *Bulletin of the Seismological Society of America* 53 (2):403–17.

Instituto Nacional de Normalización - INN. 1996. *NCh433.Of 96 Diseño sísmico de edificios*. Santiago, Chile.

Instituto Nacional de Normalización - INN. 2013. *NCh3332. Of2013 Estructuras –Intervención de construcciones patrimoniales de tierra cruda– Requisitos del Proyecto Estructural*. Santiago, Chile.

Jorquera, N. 2010. Las iglesias del altiplano: Un modelo de fusión entre el mundo hispánico y andino. In *Terra em Seminário 2010*, edited by M. Fernández, and M. Correia, 125–29. Lisboa, Portugal: Argumentum.

Kausel, E., and J. Campos. 1992. The M=8.0 tensional earthquake of December 9, 1950 of northern Chile and its relation to the seismic potential of the region. *Physics Earth Planet International* 72:220–35. doi:10.1016/0031-9201(92)90203-8.

Khazaradze, G., and J. Klotz. 2003. Short-and long-term effects of GPS measured crustal deformation rates along the south central andes. *Journal of Geophysical Research: Solid Earth* 108 (B6). doi:10.1029/2002JB001879.

Lagomarsino, S. 2006. On the vulnerability assessment of monumental buildings. *Bulletin of Earthquake Engineering* 4 (4):445–63. doi:10.1007/s10518-006-9025-y.

Lagomarsino, S. 2015. Damage assessment of churches after L'Aquila earthquake (2009). *Bulletin of Earthquake Engineering* 10 (1):73–92. doi:10.1007/s10518-011-9307-x.

Lagomarsino, S. 2015. Seismic assessment of rocking masonry structures. *Bulletin of Earthquake Engineering* 13 (1):97–128. doi:10.1007/s10518-014-9609-x.

Lagomarsino, S., and S. Podestà. 2004. Seismic vulnerability of ancient churches: I. damage assessment and emergency planning. *Earthquake Spectra* 20 (2):377–94. doi:10.1193/1.1737735.

Lagomarsino, S., S. Podestà, and S. Resemini 2004. Observational and mechanical models for the vulnerability assessment of monumental buildings. In *13th World Conference on Earthquake Engineering Vancouver*, Paper No. 942. Vancouver, BC, Canada.

Lagomarsino, S., and S. Resemini. 2009. The assessment of damage limitation state in the seismic analysis of monumental buildings. *Earthquake Spectra* 25 (2):323–46. doi:10.1193/1.3110242.

Leyton, F., S. Ruiz, and S. Sepúlveda. 2009. Preliminary re-evaluation of probabilistic seismic hazard assessment in Chile: From Arica to Taitao Peninsula. *Advances in Geosciences, Copernicus Gmbh* 22:147–53. doi:10.5194/adgeo-22-147-2009.

Leyton, F., S. Ruiz, and S. Sepúlveda. 2010. Reevaluación del peligro sísmico probabilístico en Chile central. *Andean Geology* 37 (2):455–72. doi:10.5027/andgeoV37n2-a11.

Lomnitz, C. 2004. Major earthquakes of Chile: A historical survey, 1535-1960. *Seismological Research Letters* 75 (3):368–78. doi:10.1785/gssrl.75.3.368.

Lourenco, P. 2005. Assessment, diagnosis and strengthening of Outeiro Church, Portugal. *Construction and Building Materials* 19 (8):634–45. doi:10.1016/j.conbuildmat.2005.01.010.

Lourenco, P., K. Krakowiak, F. Fernandes, and L. Ramos. 2007. Failure analysis of Monastery of Jero´nimos, Lisbon: How to learn from sophisticated numerical models. *Engineering Failure Analysis* 14 (2):280–300. doi:10.1016/j.engfailanal.2006.02.002.

Makris, N., and Konstantinidis, D. 2003. The rocking spectrum and the limitations of practical design methodologies. *Earthquake Engineering & Structural Dynamics* 32 (2):265–289.

Makris, N., and Y. Roussos. 2000. Rocking response of rigid blocks under near-source ground motions. *Geotechnique* 50 (3):243–62. doi:10.1680/geot.2000.50.3.243.

Mallardo, V., R. Malvezzi, E. Milani, and G. Milani. 2008. Seismic vulnerability of historical masonry buildings: A case study in Ferrara. *Engineering Structures* 30 (8):2223–41. doi:10.1016/j.engstruct.2007.11.006.

Martin, A. 1990. *Hacia una nueva regionalización y cálculo del peligrosísmico en Chile*. Santiago, Chile: Memoria de Titulo (unpublished), Universidad de Chile, Departamento de Ingeniería Civil, 32p.

Mauro, A., G. De Felice, and M. J. DeJong. 2015. The relative dynamic resilience of masonry collapse mechanisms. *Engineering Structures* 85:182–94. doi:10.1016/j.engstruct.2014.11.021.

Mele, E., A. De Luca, and A. Giordano. 2003. Modelling and analysis of a basilica under earthquake loading. *Journal of Cultural Heritage* 4 (4):355–67. doi:10.1016/j.culher.2003.03.002.

Ministerio de Vivienda y Urbanismo – MINVU (Chile). 2011. *Reglamento que fija el diseño sísmico de edificios y deroga D.S. N°117 MINVU of 2010*.

Ministro delle Infrastrutture e dei Trasporti – MIT (Italy). 2008. *Decreto Ministeriale 14/01/2008, Norme Tecniche per la Costruzione*. Italy.

Ministro delle Infrastrutture e dei Trasporti – MIT (Italy). 2009. *Circolare 617 del 02/02/2009, Istruzioni per l'applicazione delle nuove Norme Tecniche per le Construzioni*. Italy.

Montandón, R. 1950. *Iglesias y capillas coloniales en el Desierto de Atacama*. Santiago, Chile: Cuadernos del Consejo de Monumentos Nacionales 2, Imprenta universitaria.

Pena, M. J. 1969. *Restauración de la Iglesia y Convento de San Francisco*. París, France: UNESCO.

Pereira Salas, E. 1965. *Historia del Arte en el Reino de Chile*. Santiago, Chile: Eds. de la Universidad de Chile..

Pérez, A., J. Ruiz, G. Vargas, R. Rauld, S. Rebolledo, and J. Campos. 2014. Improving seismotectonics and seismic hazard assessment along the San Ramón Fault at the eastern border of Santiago city, Chile. *Natural Hazards* 71 (1):243–74. doi:10.1007/s11069-013-0908-3.

POLIMI (Politecnico di Milano). 2010. *Critical review of methodologies and tools for assessment of failure mechanisms and interventions_ Project 244123: New integrated knowledge based approaches to the protection of cultural heritage from earthquake-induced risk*. Milano, Italy: Politecnico di Milano.

Roca, P., M. Cervera, and G. Gariup. 2010. Structural analysis of masonry historical constructions. Classical and advanced approaches. *Archives of Computational Methods in Engineering* 17 (3):299–325. doi:10.1007/s11831-010-9046-1.

Rodríguez, H. 2012. Iglesias de Atacama. Nueva arquitectura para antiguas creencias. In *Atacama*, edited by C. A. Del Solar, 158–97. Santiago, Chile: Museo Chileno de Arte Precolombino.

Romanoff, F. 1999. *Estudio del Peligro Sísmico en la Región Metropolitana*. Santiago, Chile: Memoria de Titulo (unpublished), Universidad de Chile, Departamento de Ingeniería Civil, 85 p.

Rovegno, J. R. 2009. *La casa de fray Pedro de Bardeci. El convento de San Francisco. Santiago de Chile. Ensayo cronológico 1554-2004*. Santiago, Chile: Ediciones Alameda, Orden franciscana de Chile..

Rovero, L., V. Alecci, J. Mechelli, U. Tonietti, and M. De Stefano. 2015. Masonry walls with irregular texture of L'Aquila (Italy) seismic area: Validation of a method for the evaluation of masonry quality. *Materials and Structures* 49 (6):2297–314. doi:10.1617/s11527-015-0650-2.

Rovero, L., and F. Fratini. 2013. The Medina of Chefchaouen (Morocco): A survey on morphological and mechanical features of the masonries. *Construction and Building Materials* 47:465–79. doi:10.1016/j.conbuildmat.2013.05.025.

Rovero, L., and U. Tonietti. 2012. Structural behavior of earthen corbelled domes in the Aleppo's region. *Materials and Structures* 45 (1):171–84. doi:10.1617/s11527-011-9758-1.

Rovero, L., and U. Tonietti. 2014. A modified corbelling theory for domes with horizontal layers. *Construction and Building Materials* 50:50–61. doi:10.1016/j.conbuildmat.2013.08.032.

Sahady, A. 2015. *Mutaciones del patrimonio arquitectónico de Santiago de Chile. Una revisión del centro histórico*. Santiago, Chile: Editorial Universitaria.

Sani, F., G. Moratti, M. Coli, P. Laureano, L. Rovero, U. Tonietti, and N. Coli. 2012. Integrated geological-architectural pilot study of the Biet Gabriel-Rufael rock hewn church in Lalibela, northern Ethiopia. *Italian Journal of Geosciences* 131 (2):171–86.

Scholz, C. H. 2002. *The mechanics of earthquakes and faulting*. Cambridge, UK: Cambridge university press.

Shawa, O. A., G. Felice, A. Mauro, and L. Sorrentino. 2012. Out-of-plane seismic behaviour of rocking masonry walls. *Earthquake Engineering & Structural Dynamics* 41 (5):949–68. doi:10.1002/eqe.1168.

Shenton III, H. W. 1996. Criteria for initiation of slide, rock, and slide-rock rigid-body modes. *Journal of Engineering Mechanics* 122 (7):690–93. doi:10.1061/(ASCE)0733-9399(1996)122:7(690).

Sorrentino, L., O. AlShawa, and L. D. Decanini. 2011. The relevance of energy damping in unreinforced masonry rocking mechanisms. Experimental and analytic investigations. *Bulletin of Earthquake Engineering* 9 (5):1617–42. doi:10.1007/s10518-011-9291-1.

Sorrentino, L., D. D'Ayala, G. De Felice, M. C. Griffith, S. Lagomarsino, and G. Magenes. 2016. Review of out-of-plane seismic assessment techniques applied to existing

masonry buildings. *International Journal of Architectural Heritage* 1–20. doi:10.1080/15583058.2016.1237586.

Sorrentino, L., S. Kunnath, G. Monti, and G. Scalora. 2008. Seismically induced one-sided rocking response of unreinforced masonry façades. *Engineering Structures* 30 (8):2140–53. doi:10.1016/j.engstruct.2007.02.021.

Strand, 7. 2004. *Straus 7.2: User's manual*. Sidney, Australia: Strand 7. www.strand7.com.

Villalobos, S., L. Méndez, C. Canut De Bon, S. Pinto, S. Serrano, L. Parentini, L. Ortega, E. Cavieres, R. Sagredo, and J. Plass. 1990. *Historia de la ingeniería en Chile*. Santiago, Chile: Hachette.

Vukasovic, Ruz, Ltda. 2013. *Informe de mecánica de suelo. Museo histórico nacional Plaza de Armas, Comuna de Santiago, Región Metropolitana, Chile*. Santiago, Chile: Vukasovic, Ruz, Ltda..

Yim, C.-S., A. K. Chopra, and J. Penzien. 1980. Rocking response of rigid blocks to earthquakes. *Earthquake Engineering and Structural Dynamics* 8 (6):565–87. doi:10.1002/eqe.4290080606.